

# III –V Quantum Structures for Infrared Detection

Sarath Gunapala

NASA - Jet Propulsion Laboratory  
California Institute of Technology  
Pasadena, California  
USA

September 5, 2017

Copyright 2017 California Institute of Technology. U.S. Government sponsorship acknowledged.

# Center of Infrared Photodetectors Capabilities



- Concept, theory, design, and analysis
- Material growth and characterization
- Process development
- Detector fabrication
- Detector characterization
- Array fabrication
- FPA characterization
- IDCA and camera

JPL's in-house capability provides end-to-end development of III-V IR FPAs  
- From quantum mechanics to infrared imagers

- Introduction
- Quantum well infrared photodetectors (QWIPs)
- InAs/GaSb superlattices for MWIR and LWIR detection
- Applications



# Introduction



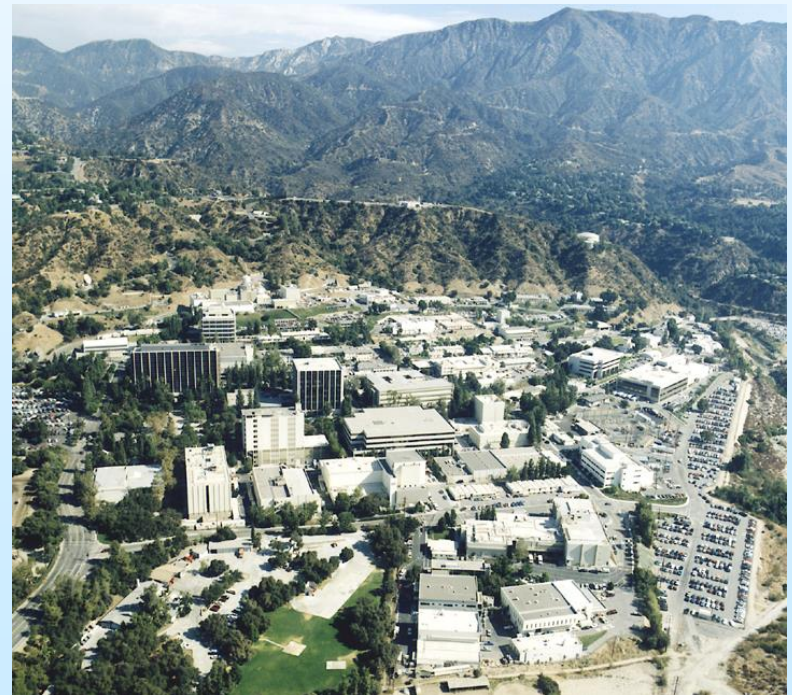
# Jet Propulsion Laboratory

Jet Propulsion Laboratory  
California Institute of Technology



- JPL is a child of Caltech: founded in 1936 as a graduate student project under Professor Theodore von Kármán.
- JPL led the development of US rocket technology in WWII.
- Developed the first U.S. satellite, Explorer I.
- JPL was transferred to NASA upon its creation in 1958.
- JPL spacecraft have explored all the planets of the solar system except Pluto.

- About JPL:
  - A Federally-Funded Research and Development Center (FFRDC) under NASA sponsorship;
  - A division of Caltech, staffed with ~5,000 – 10,000 Caltech employees;
  - JPL Director is a Vice-President of Caltech.
- Programs:
  - NASA programs;
  - Defense programs and civilian programs of national importance compatible with JPL capabilities.

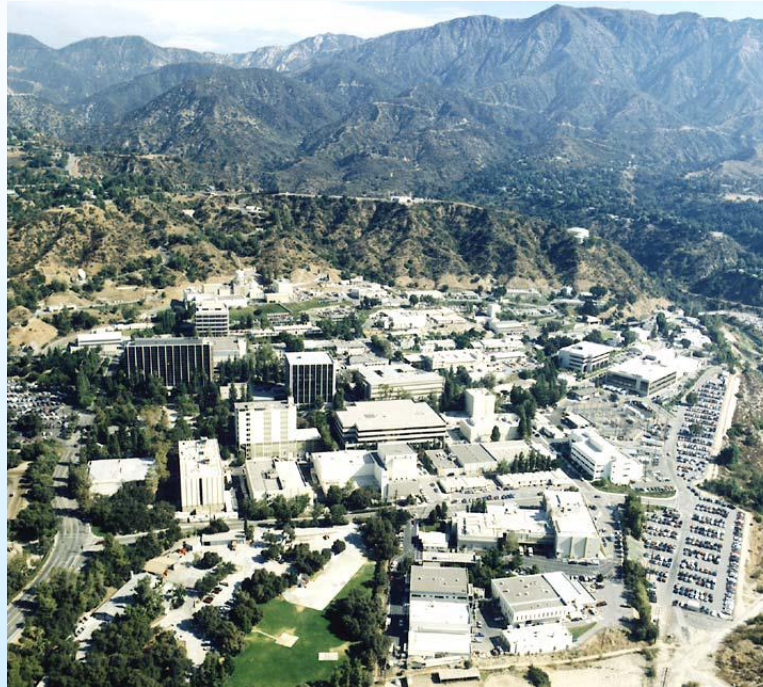




# A little about JPL .....



1936



JPL Today



1940



1958



1950



# Brief Introduction to Infrared

# Discovery of Infrared

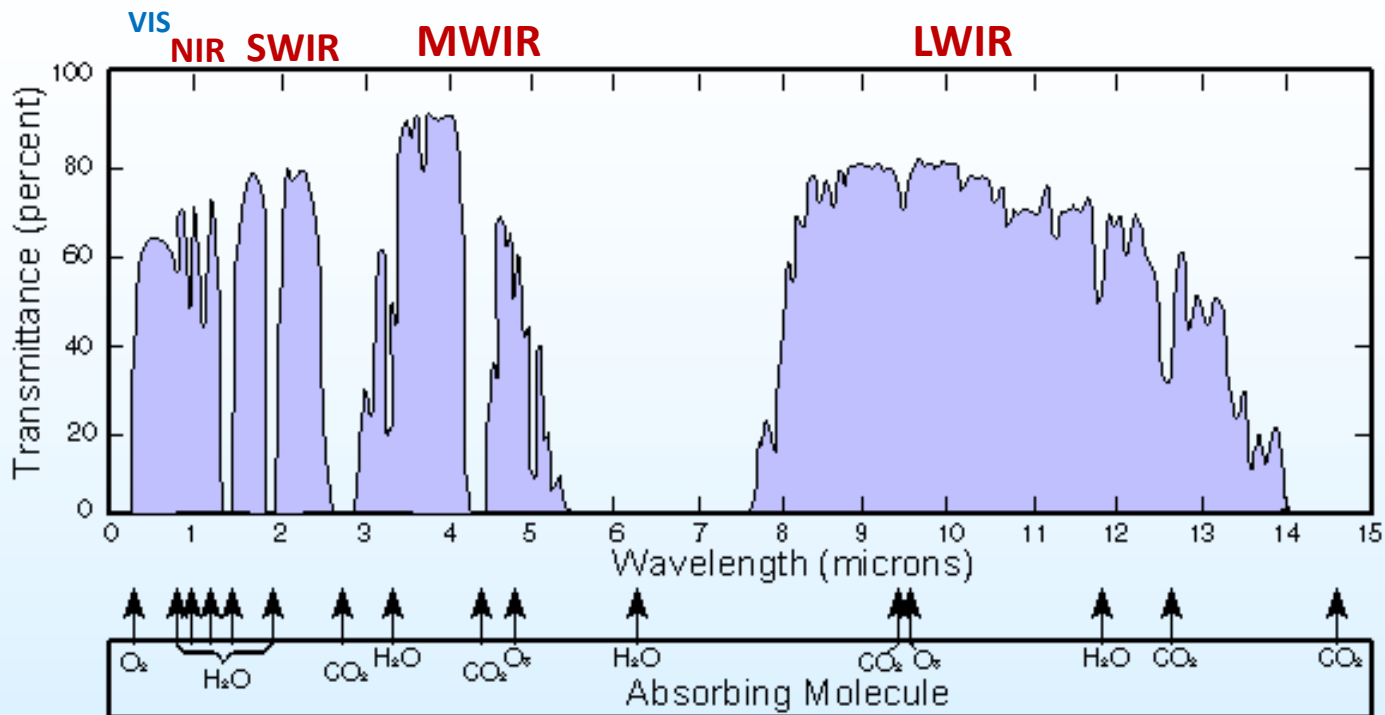


[http://coolcosmos.ipac.caltech.edu/cosmic\\_classroom/ir\\_tutorial/discovery.html](http://coolcosmos.ipac.caltech.edu/cosmic_classroom/ir_tutorial/discovery.html)

[http://en.wikipedia.org/wiki/William\\_Herschel](http://en.wikipedia.org/wiki/William_Herschel)

- Sir Frederick William Herschel
  - Musician and composer
  - Built and sold large telescopes
  - Discovered Uranus and 2 of its moons; 2 Saturn moons; double stars
  - Surveyed and catalogued deep sky objects – nebulae, clusters
- Discovered infrared on Feb. 11, 1800
  - Testing filters for sunspot observations
    - Red filter retained more heat
  - Passed sunlight through prism
  - Measured temperatures for color spectrum
    - Increasing from violet to red
  - Placed thermometer just beyond red; showed higher temperature than visible!
  - Invisible form of light – “calorific rays”
    - Reflected, refracted, absorbed, transmitted
  - Postscript: Led to discovery of ultra-violet light by Johann Ritter in 1801
    - “Chemical rays” (reaction in silver chloride)

# Atmospheric Transmittance and Infrared Bands



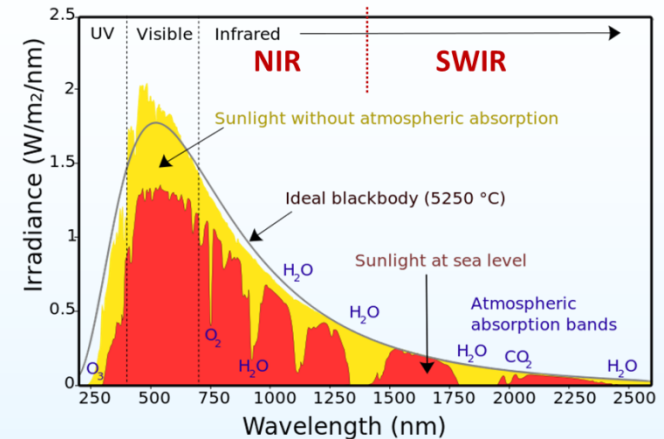
<http://en.wikipedia.org/wiki/Infrared>

- Near-infrared (NIR): 0.75 – 1.7  $\mu\text{m}$
- Short-wavelength infrared (SWIR): 1.7 - 3  $\mu\text{m}$
- Mid-wavelength infrared (MWIR): 3 – 5.5  $\mu\text{m}$
- Long-wavelength infrared (LWIR): 8 - 12  $\mu\text{m}$
- Beyond: Very Long-wavelength infrared (VLWIR), Far IR (FIR)
- Different convention for Astronomy: Near-IR, Mid-IR, Far-IR

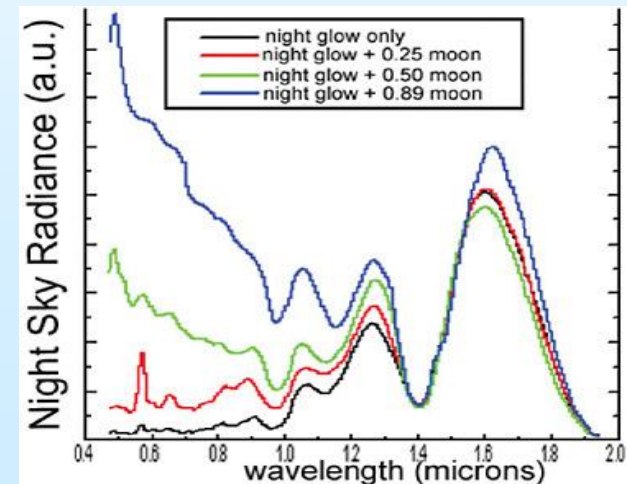
# Common Sources of Infrared Light

- Reflected infrared
  - Like reflected visible light
  - Sunlight (NIR, SWIR)
    - Solar spectrum at sea level: 4% UV, 44% Visible, 52% IR
  - Airglow/Atmospheric Nightglow (SWIR)
    - Night time emission from the Earth's upper atmosphere
    - Mostly in SWIR
- Emitted infrared
  - Blackbody radiation (MWIR, LWIR)
    - 300K BB spectral peak  $\sim 9.7 \mu\text{m}$

Spectrum of Solar Radiation (Earth)



[http://commons.wikimedia.org/wiki/File:Solar\\_spectrum\\_ita.svg](http://commons.wikimedia.org/wiki/File:Solar_spectrum_ita.svg);  
 By Nick84 [CC BY-SA 3.0 (<http://creativecommons.org/licenses/by-sa/3.0/>)], via Wikimedia Commons



SOURCE: Vatsia, L.M. 1972. Atmospheric optical environment. Research and Development Technical Report ECOM-7023. Prepared for the Army Night Vision Lab, Fort Belvoir, Va.

# The First Infrared Image



[http://benbeck.co.uk/firsts/1\\_Technology/invisible.htm](http://benbeck.co.uk/firsts/1_Technology/invisible.htm)

- First infrared photographs were taken by American physicist Robert Williams Wood in October 1910.
  - Wood was also the first to photograph in the ultraviolet
  - Trees look unusual
  - Upper sky looks dark

# Near IR Image: Sky and Leaves

Visible



(Reflected) Near IR



By Dschwen (Own work) [CC BY-SA 2.5 (<http://creativecommons.org/licenses/by-sa/2.5>)], via Wikimedia Commons  
[http://en.wikipedia.org/wiki/Infrared\\_photography](http://en.wikipedia.org/wiki/Infrared_photography)

- Why is the overhead sky dark in the near-IR?
  - For the same reason the sky is blue in the visible
  - Weaker Rayleigh Scattering ( $1/\lambda^4$ ) of longer wavelength sunlight
- Why are the leaves and grass bright in the near-IR?
  - Leaves absorb red and blue light, but reflect green and near-IR light.
  - So leaves look bright in the NIR. Wood Effect. Monitor plant health.

# Human Images: (Reflected) Visible, NIR, SWIR

Visible

NIR

NIR/SWIR



Visible (400-700nm)



Near IR (750-900nm)



SWIR (1500-1700nm)

"Infrared portrait comparison" by NickSpiker - Own work. Licensed under CC BY-SA 4.0 via Wikimedia Commons -  
[http://commons.wikimedia.org/wiki/File:Infrared\\_portrait\\_comparison.jpg#mediaviewer/File:Infrared\\_portrait\\_comparison.jpg](http://commons.wikimedia.org/wiki/File:Infrared_portrait_comparison.jpg#mediaviewer/File:Infrared_portrait_comparison.jpg)  
[http://en.wikipedia.org/wiki/Infrared#Hyperspectral\\_imaging](http://en.wikipedia.org/wiki/Infrared#Hyperspectral_imaging)

- **SWIR Imaging**
  - Skin looks dark (high moisture content)
    - SWIR penetrates into the skin, absorbed
  - Hair looks white (lack of moisture)



# Introductions to Quantum Well Infrared Detectors

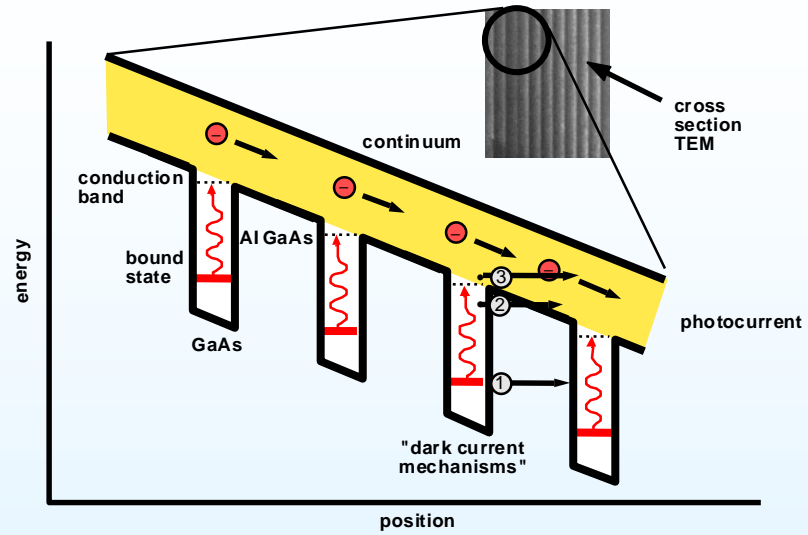
## In the Beginning ...

- Proposal of superlattices and quantum wells in 1977
  - L. Esaki and H. Sakaki, IBM Tech. Disc. Bull. 20, 2456, 1977
  - D. D. Coon *et al.*, Appl. Phys. Lett. 45, 649, 1984.
  - L. C. West and S. J. Eglash, (1985). Appl. Phys. Lett. 46, 1156, 1985.
    - Proposed quantum wells for infrared detection (theory)
    - Intersubband absorption in GaAs/AlGaAs quantum well were observed in 1985
- First demonstration of infrared detection using quantum wells in 1988
  - B. F. Levine *at al.*, Appl. Phys. Lett. **53**, 231, 1988.
  - B. F. Levine *et al.*, Appl. Phys. Lett., **53**, 296, 1988.
    - Challenge the industry state-of-art HgCdTe for the first time
    - Over 40 groups were working on QWIPs in early nineties

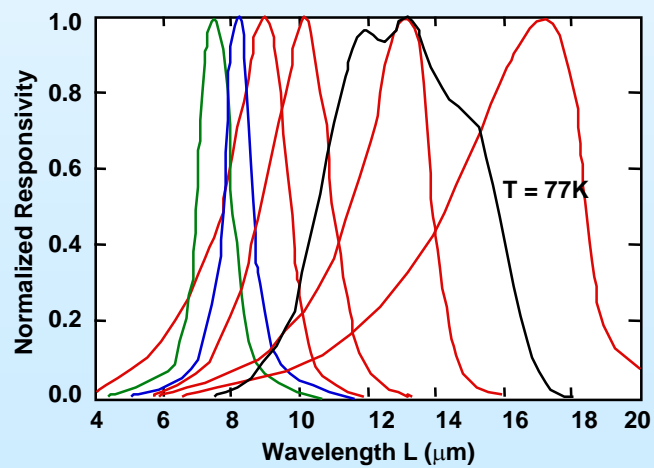


# III-V Crystal Growth at JPL.....

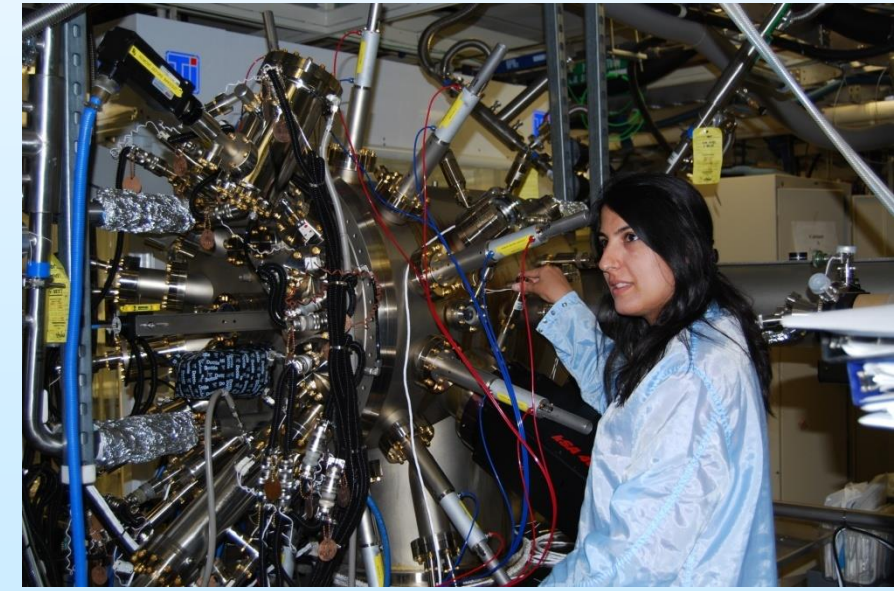
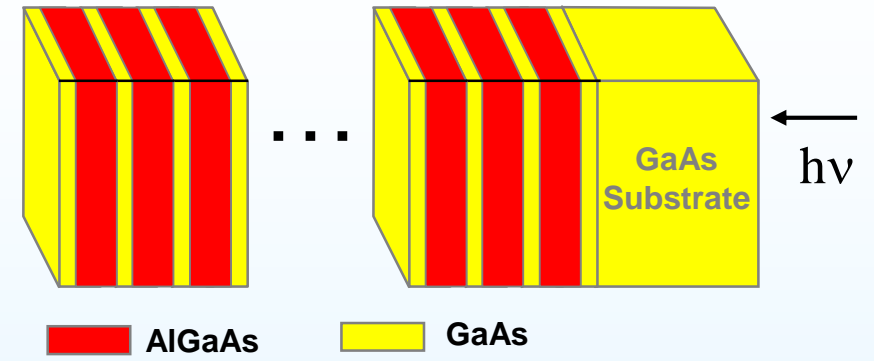
Jet Propulsion Laboratory  
California Institute of Technology



QWIP Band Diagram

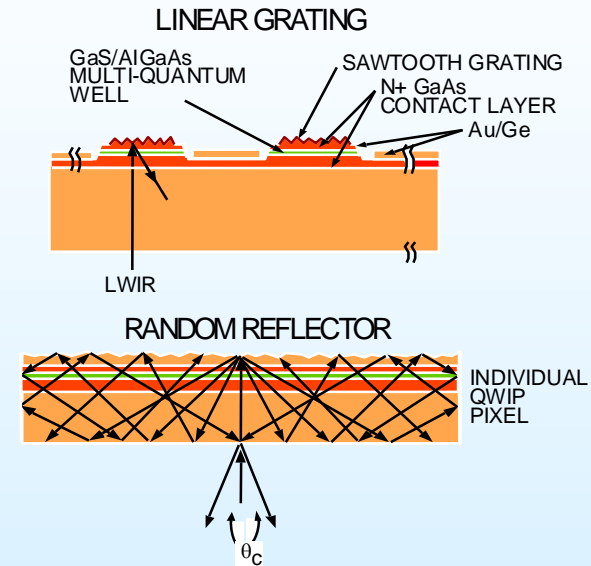
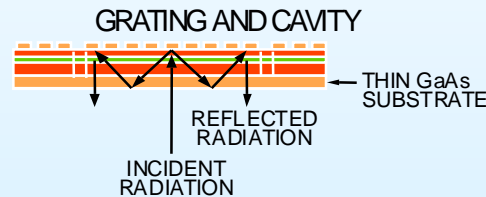
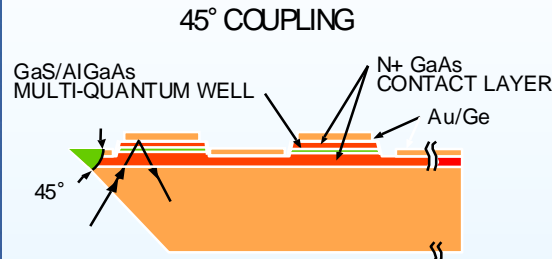
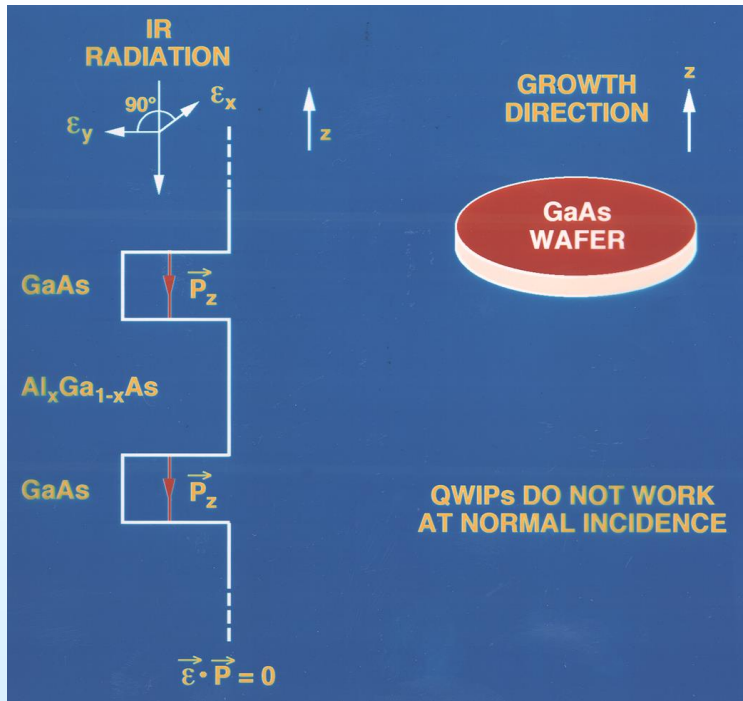


GaAs/AlGaAs Based QWIP Can Cover a Very Broad Infrared (3-25  $\mu\text{m}$ ) Region



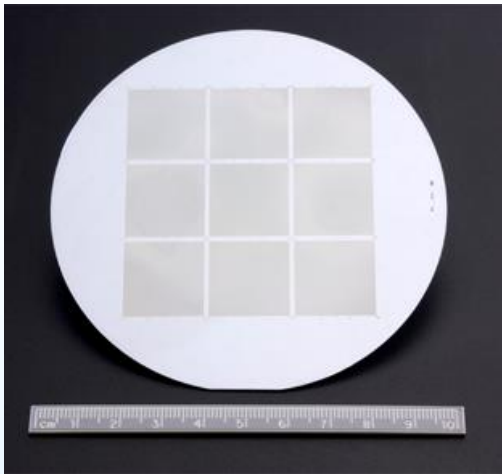
Veeco 4-inch capable GEN-III Molecular Beam Epitaxy Growth Machine

# Key Technical Issues

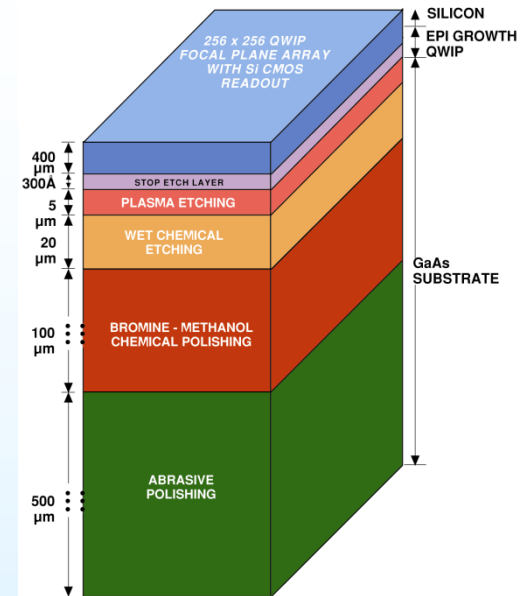


Why QWIPs Do Not Work with Normal Incident Light? Need Light Coupler such as gratings.

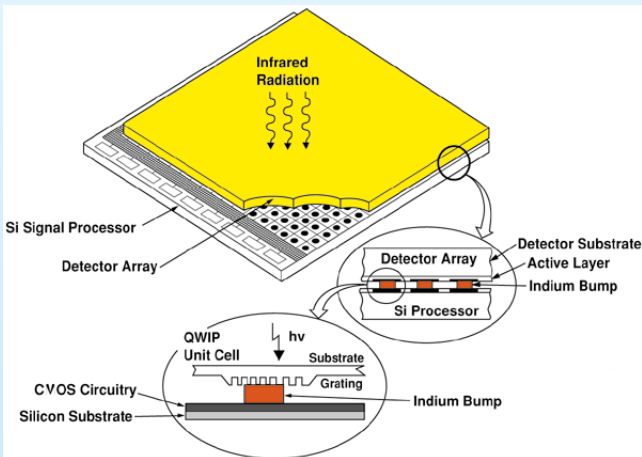
# Focal Plane Array Fabrication Process



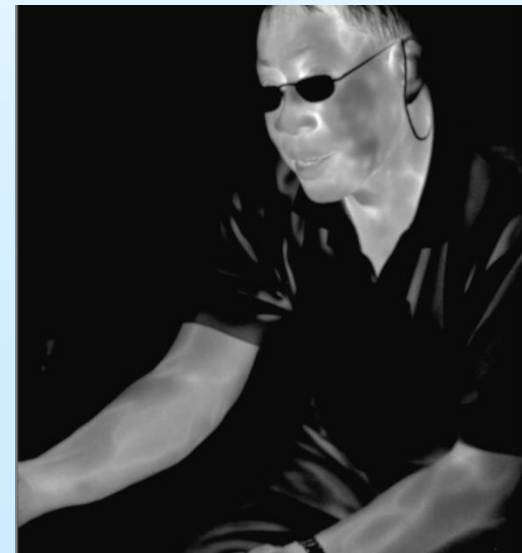
**Nine 1024 x 1024 QWIP  
Focal Plane Arrays (FPAs)  
on 4-inch GaAs Wafer**



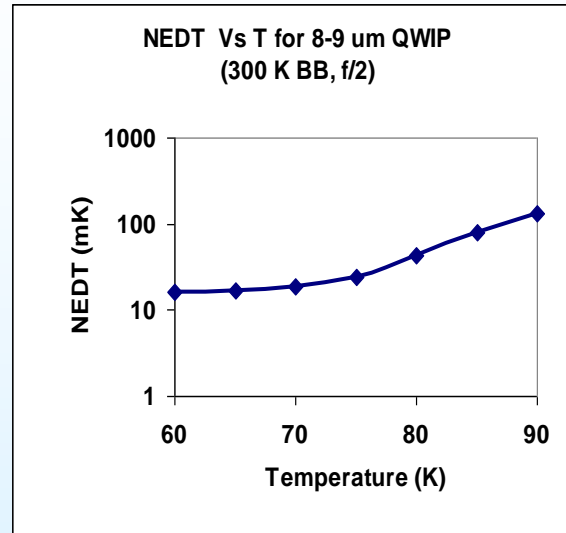
**FPA Thinning Process**



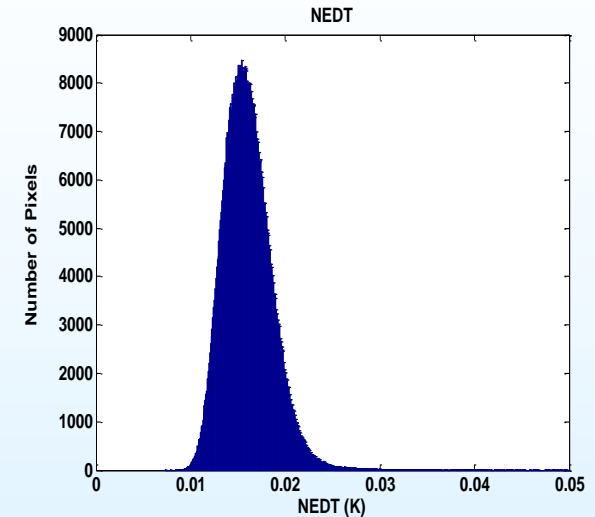
**Indium Bump Bonding Process**



# 1024x1024 Pixel LWIR QWIP FPA



NOISE EQUIVALENT TEMPERATURE DIFFERENCE



NOISE EQUIVALENT TEMPERATURE DIFFERENCE HISTOGRAM

- Wavelength - 8-9  $\mu\text{m}$
- Net quantum efficiency - 3.0%
- NE $\Delta$ T - 16 mK
- Pixel pitch - 19.5  $\mu\text{m}$
- Pixel operability - 99.8%
- Operating temperature - 72K

# QWIP Cameras for IR imaging.....



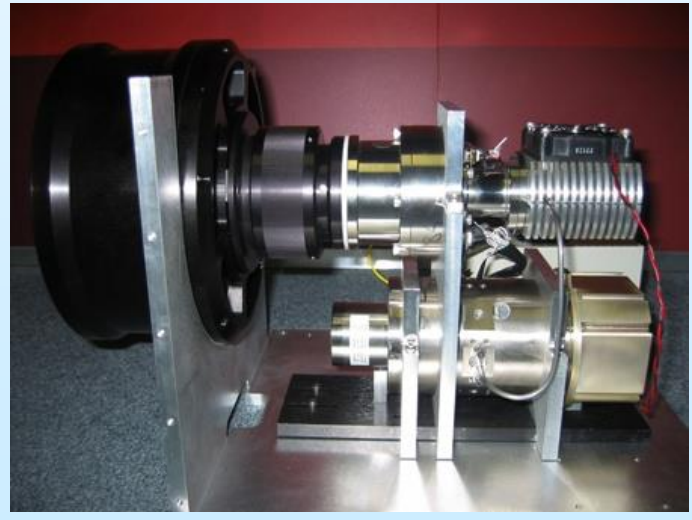
Palm-size with 256x256 FPA



Hand-held with 320x256 FPA

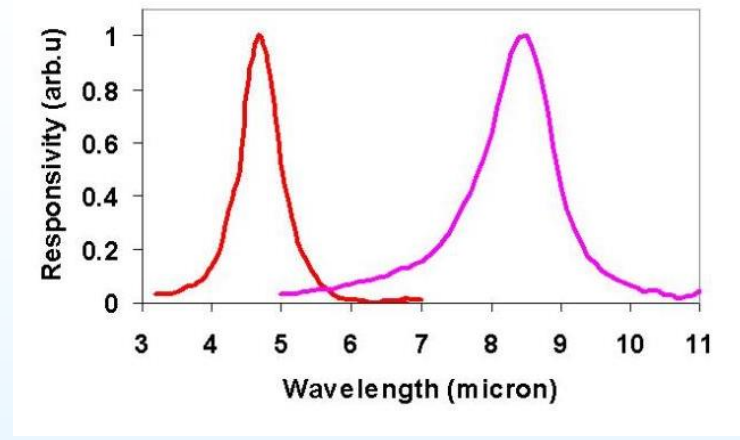
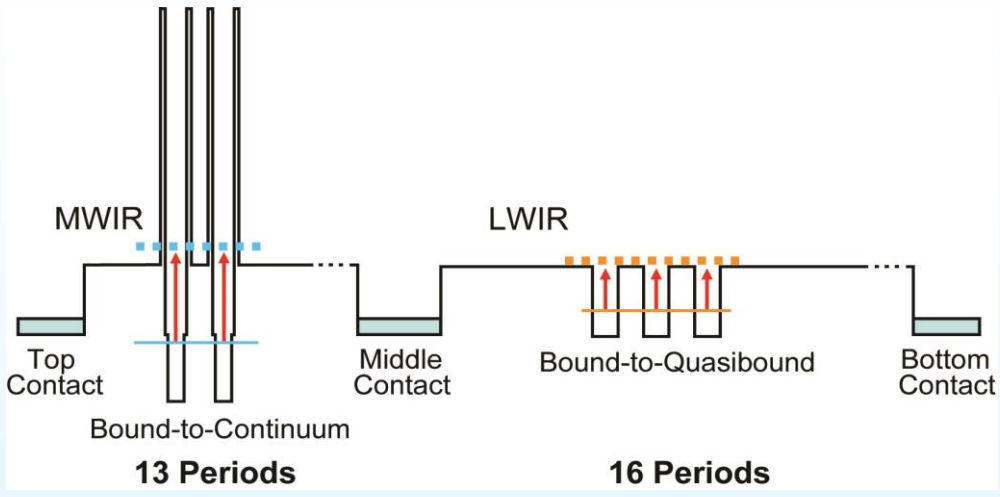


Hand-held with 640x512 FPA



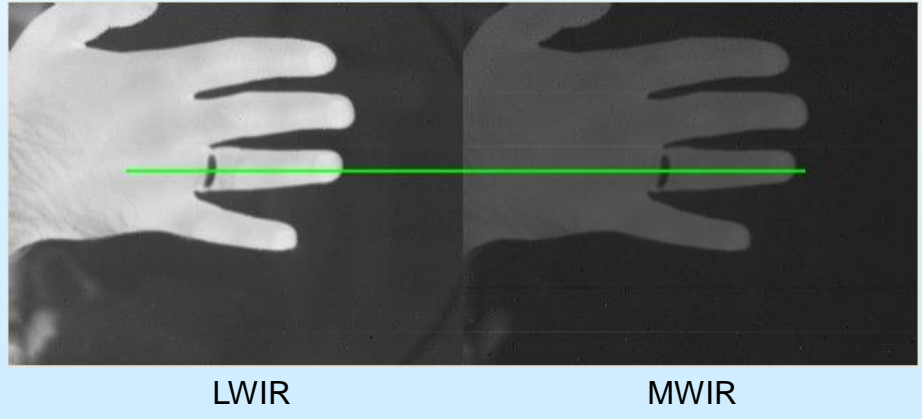
Desk-top with 640x512 dual-broadband FPA

# Pixel Co-Registered Simultaneously Readable Dual-band QWIP Pixel

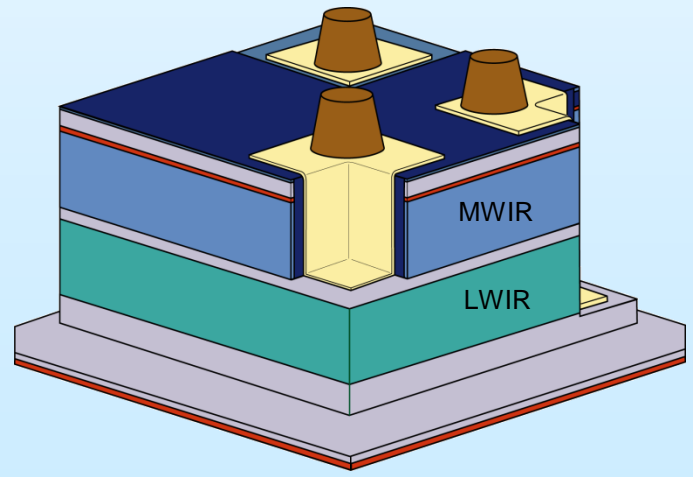


Dual-band responsivity spectrum

Dual-band device structure



Could be use for measurement for absolute  
temperature of objects remotely

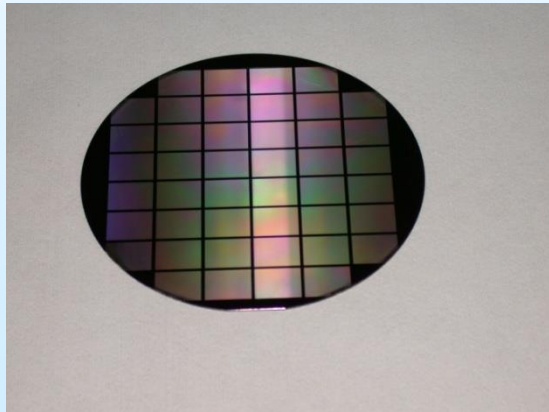


Dual-band pixel architecture

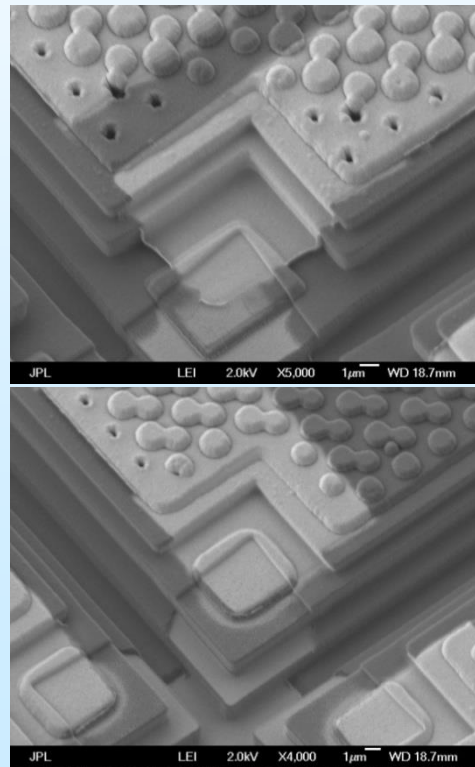


# Dual-band Pathfinder Detector Array

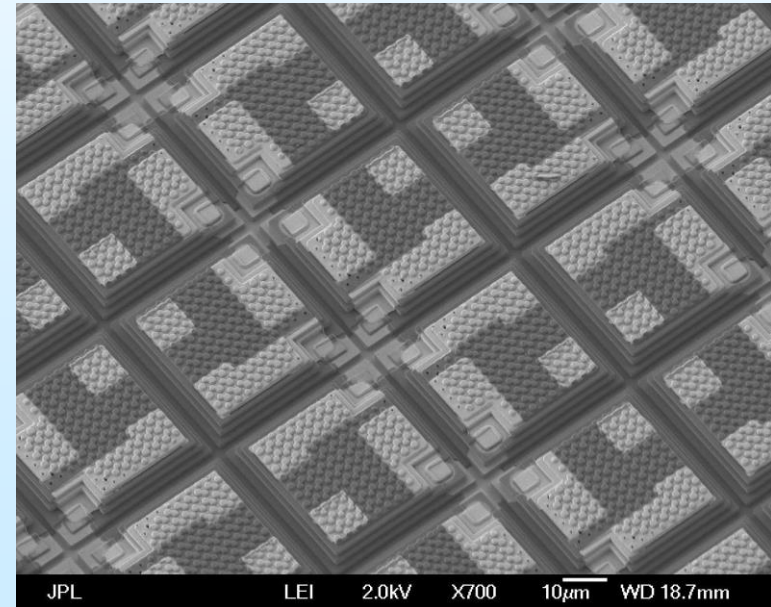
- Features well aligned (320x256 pixels)
- Thin device structure
- New via architecture allows more net space in via hole
- Completely new processing scheme
- SEMs show clear via connections and pixel isolation trenches
- Pixels are electrically not shorted or open



4-inch wafer with 48  
detector dies



ZZ

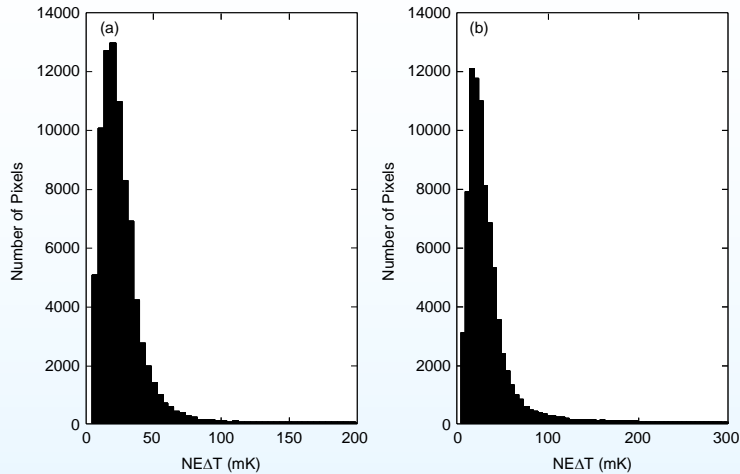


SEM of dualband QWIP array



# Imagery with Dual-band QWIP Pathfinder Array

Jet Propulsion Laboratory  
California Institute of Technology



LWIR

MWIR

The experimentally measured NE $\Delta$ T of MWIR and LWIR detectors at 65 K are 28 and 38 mK, respectively.

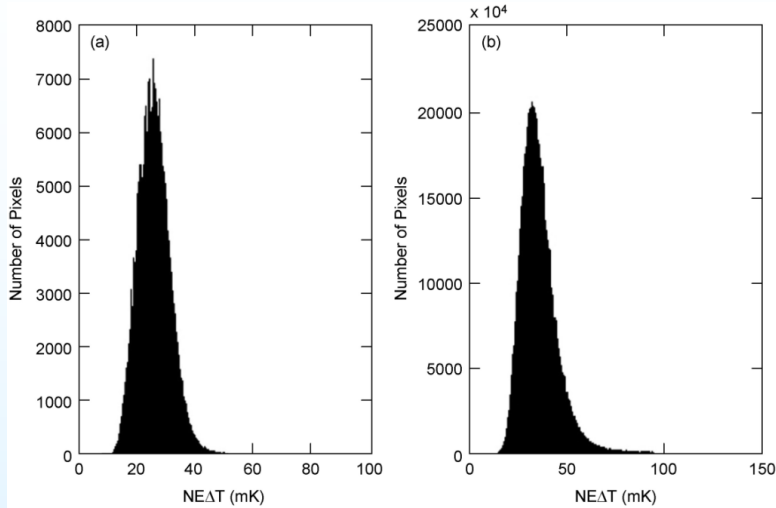
## Features to look for.

The cigarette lighter produce lots of hot CO<sub>2</sub> gas. So, flare is broader MWIR due to CO<sub>2</sub> emission, where as LWIR (8-9 microns) doesn't have any emission (just the heat).  
 The hot cigarette lighter flame produce so much MWIR signal, it reflects off from the lens and Jason's face.  
 The plastic piece Jason is holding is opaque in LWIR, but transparent in MWIR.

Format	- 320x256 pixels, dualband & pixel co-registered
Wavebands	- 4.4-5.1 & 8-9 $\mu$ m
NE $\Delta$ T	- 28 & 38 mK for 300K background with f/2 optics
Net QE	- 3.8% & 3%
Detectivity	- > 2x10 <sup>11</sup> & 1x10 <sup>11</sup> Jones
Operating temp.	- 65 K
Fill factor	- > 81%



# First Megapixel MW/LW Dual-band QWIP



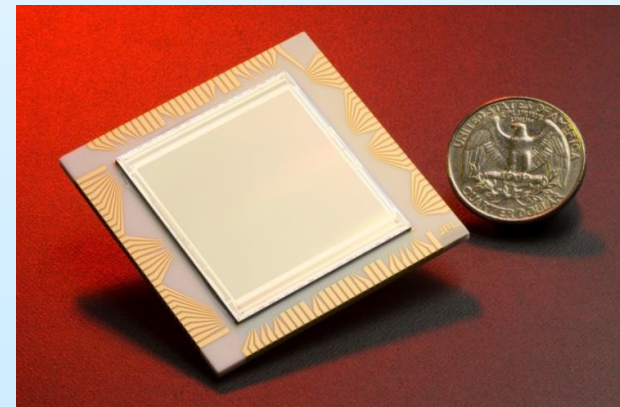
MWIR

LWIR



Flame in MWIR image (left panel) looks broader due to the detection of re-emitted infrared signal from the heated CO<sub>2</sub> gas produced by the cigarette lighter in 4.1-4.3 μm band.

NEΔT	- 27 & 40 mK for MWIR & LWIR
Operability	- 90% (full frame)
Operability	- 99% & 97.5%
Net QE	- 3.8% & 3%
Detectivity	- > 2x10 <sup>11</sup> & 1x10 <sup>11</sup> Jones
Op. temp.	- 65 K
Fill factor	- 76% & 81%



Megapixel dual-band ROIC on 124 pin LCC  
Pixel pitch – 30 μm

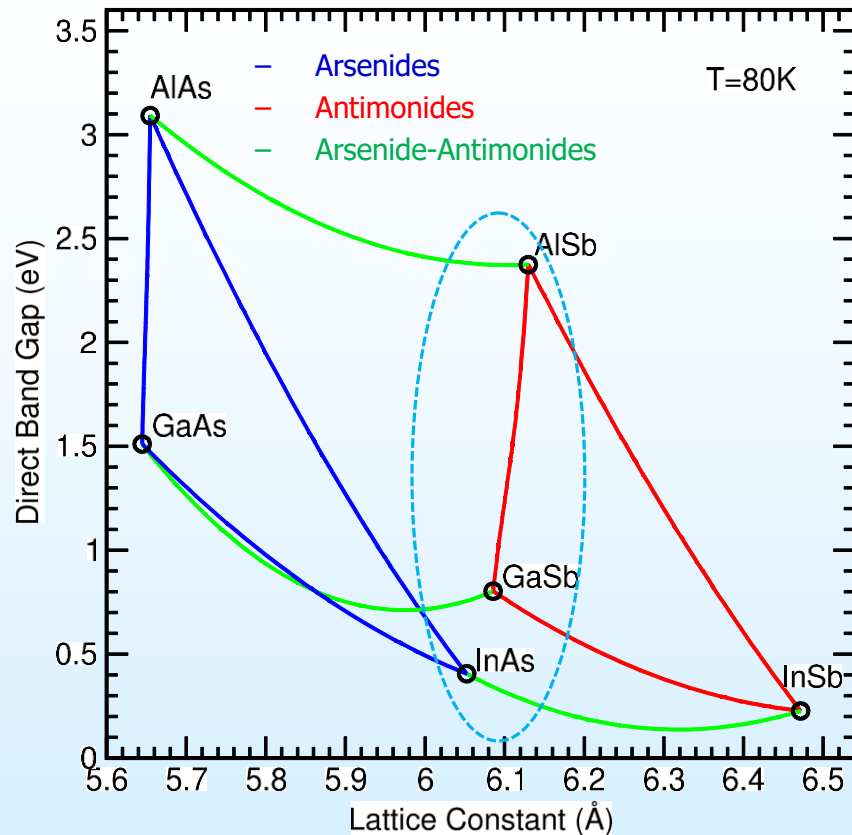


# Introductions to Antimonides for Infrared Detection.....

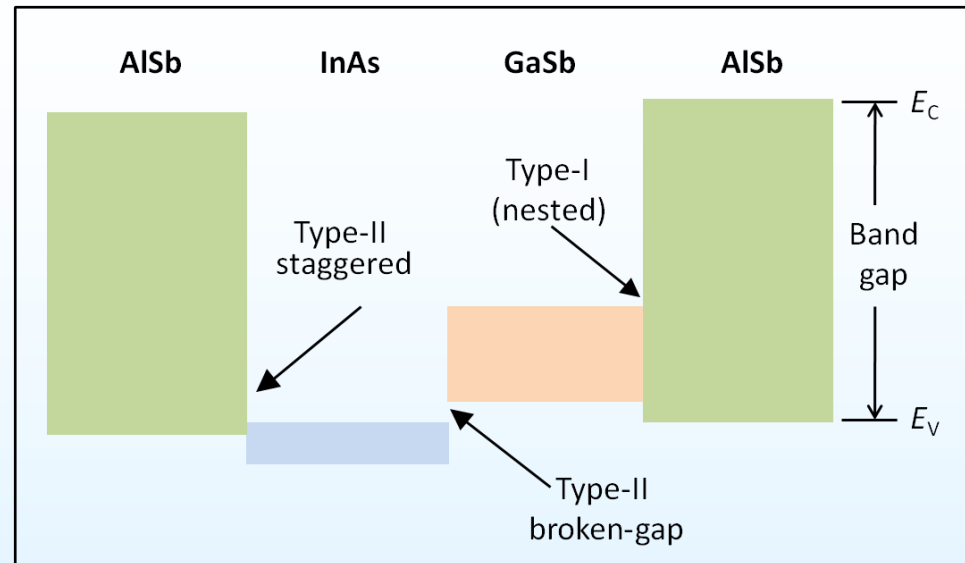
## In the Beginning ...

- Discovery of the broken-gap band alignment between InAs and GaSb in 1977
  - W. Frensley Thesis, U. Colorado (Advisor: Kroemer)
  - G. Sai-Halasz *et al.*, IBM, based on electron affinity rule
  - Frensley and Kroemer, UCSB, pseudopotential theory
    - Commented that, among all predicted band offsets, the broken gap alignment between InAs and GaSb is the most interesting
- Theoretical prediction of type-II superlattice in 1977
  - “A new semiconductor superlattice”, Sai-Halasz, G. A., Tsu, R., and Esaki, L. *Appl. Phys. Lett.* **30**, 651 (1977).
  - Demonstrated experimentally by the same group in 1978

# Antimonides Material System for Type-II Superlattices



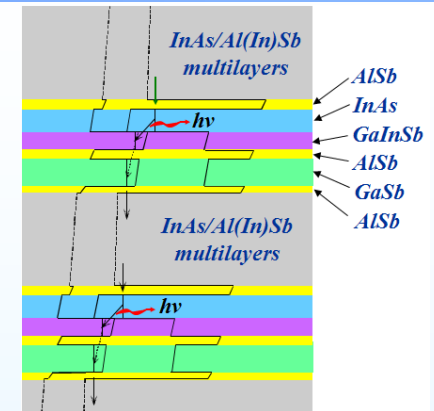
- Material system includes InAs, GaSb, AISb and their alloys
  - Nearly lattice matched ( $\sim 6.1 \text{ \AA}$ )
- Alloys with GaAs, AlAs, and InSb adds even more flexibility



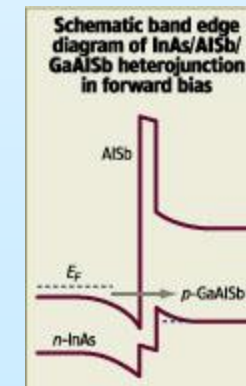
- Three types of band alignments
  - Type-I (nested, straddling)
  - Type-II staggered
  - Type-II broken gap (misaligned, Type-III)
    - Unique among common semiconductor families
    - Overlap between InAs CB and GaSb VB enables interband devices
- Tremendous flexibility in artificially designed materials / device structures

# Antimonide Devices

- Resonant tunneling diode (RTD) and resonant **interband** tunneling diode (RITD)
- Antimonide-based high-electron mobility transistor (HEMT) and heterojunction bipolar transistor (HBT)
  - High-frequency operation with much lower power consumption than GaAs and InP based devices
- GaSb based thermophotovoltaics (TPV)
- High-power 2-3  $\mu\text{m}$  lasers
  - Fraunhofer, Montpelier, Sarnoff, MIT, Stony Brook, ...
- JPL (Prof. Rui Yang) 3.27  $\mu\text{m}$  **interband** cascade laser (ICL) in a tunable laser spectrometer (TLS)
  - For methane detection on Mars
- Type-II **interband** heterostructure backward diode (Schulman diode, HRL)
  - Highly sensitive detectors essential for passive mm-wave detection imaging cameras, produced by Trex Enterprises, Millivision, Brijou,...
- Spintronic devices and quantum spin Hall effect
- MWIR/LWIR photodetectors (JPL, NRL, Columbia, UCSB, NWU, ARL, ..... )
  - **Type-II** superlattice



JPL (Rui Yang) interband cascade laser in Mars Science Laboratory (2011 launch)



Interband heterostructure backward diode for passive mm-wave detection.

# Material Robustness

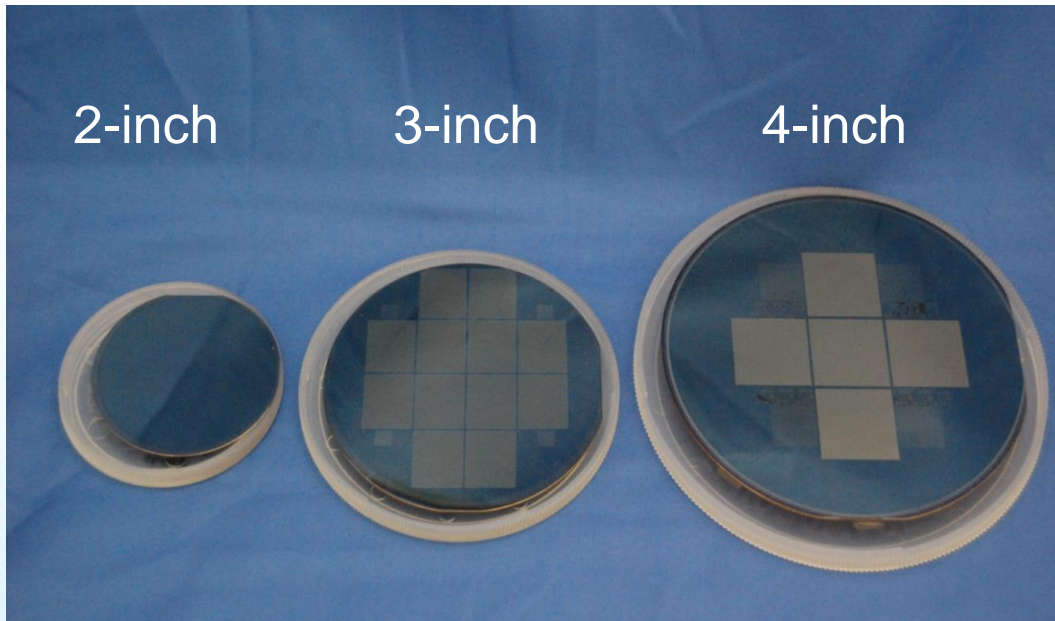
## Semiconductor Families for Infrared Photodetection

	Si	Ge	GaAs	AlAs	InP	InGaAs	AlInAs	InAs	GaSb	AlSb	InSb	HgTe	CdTe
<b>Group</b>	IV	IV	III-V	III-V	III-V	III-V	III-V	III-V	III-V	III-V	III-V	II-VI	II-VI
<b>Lattice Constant [Å]</b>	5.431	5.658	5.653	5.661	5.870	5.870	5.870	6.058	6.096	6.136	6.479	6.453	6.476
<b>Bulk Modulus [Gpa]</b>	98	75	75	74	71	69	66	58	56	55	47	43	42
<b>Direct Gap [eV] (λ [μm])</b>	-	-	1.426 (0.87)	-	1.350 (0.92)	0.735 (1.69)	-	0.354 (3.5)	0.730 (1.7)	-	0.175 (7.1)	-0.141	1.475
<b>MWIR/LWIR Detection Mechanism</b>	Heterojunction Internal photoemission (HIP)		Quantum well/dot Intersubband (QWIP/ QDIP)		Quantum well Intersubband (QWIP)			Bulk (MW) / Superlattice (MW/LW) Band-to-Band			Bulk B-B	Bulk Band-to-Band	

## General Trends

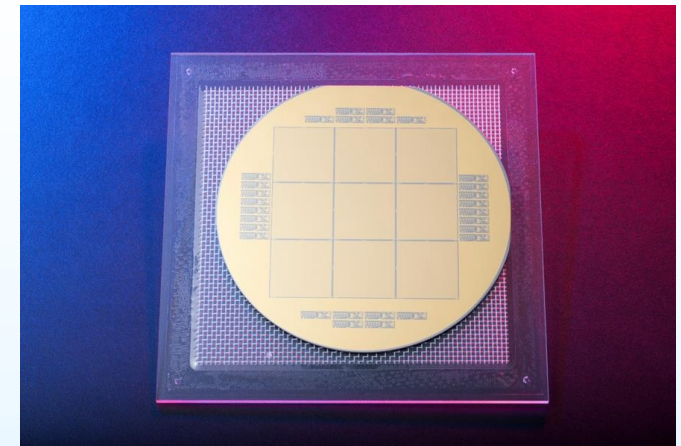
- Larger lattice constant
- Weaker chemical bond (less covalent)
- Decreasing material robustness / manufacturability
- Smaller band gap (enables strong band-to-band IR absorption)
- Higher quantum efficiency

# GaSb Substrates



Side-by-side comparison of 2-inch, 3-inch (with 640x512 arrays), and 4-inch (with 1k x 1k arrays and test devices) GaSb wafers

- Substrates with relatively large diameters
  - InAs: 2-inch and 3-inch diameter
  - GaSb: 2-inch, 3-inch and 4-inch diameter
  - Quality improving with demand
  - MBE growth of Sb-based infrared photodetector structures on 6-inch GaSb substrates, Amy W. K. Liu, et al. *Proc. SPIE* 9451, Infrared Technology and Applications XLI, 94510T (June 4, 2015); doi:10.1117/12.2178122



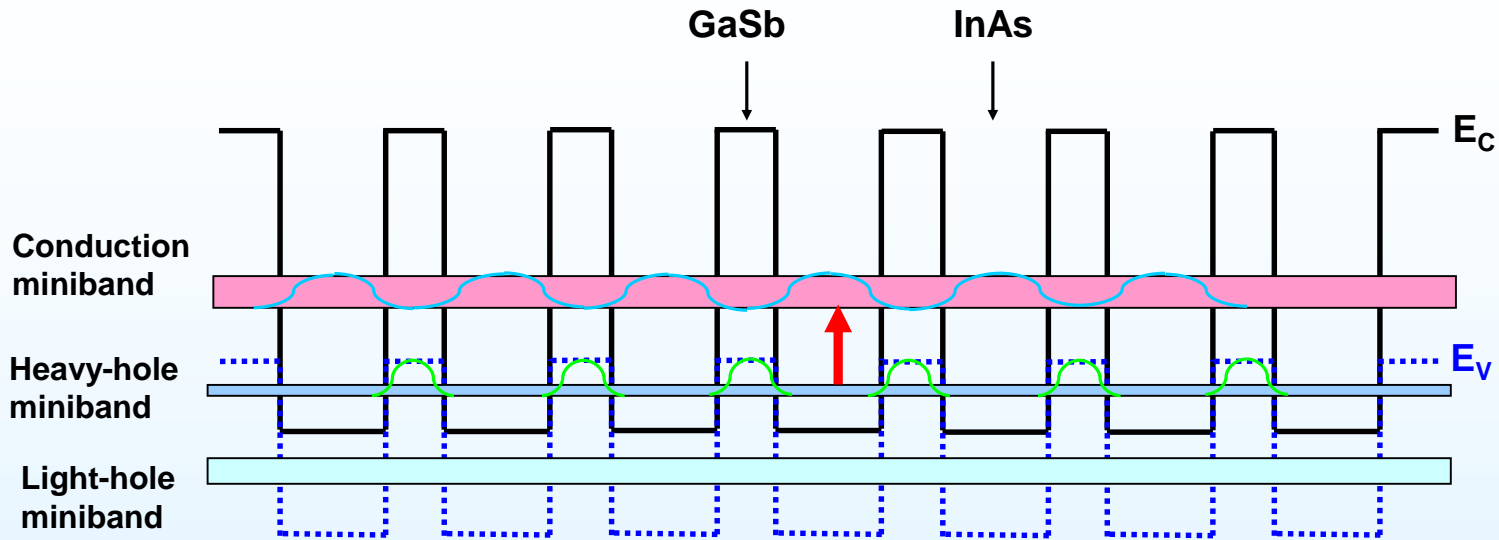
4-inch GaSb wafer with nine 1K x 1K arrays and test devices

# Early History of Superlattice IR Detectors

Caltech Solid-State Device Physics Group – T. C. McGill

- J. N. Schulman and T. C. McGill, “The CdTe/HgTe superlattice: Proposal for a new infrared material,” *Appl. Phys. Lett.* **34**(10), 663 (1979).
- D. L. Smith, T. C. McGill, and J. N. Schulman, “Advantages of the HgTe-CdTe superlattice as an infrared detector material,” *Appl. Phys. Lett.* **43**(2), 180 (1983).
- D. L. Smith and C. Mailhot, “Proposal for strained type II superlattice infrared detectors,” *J. Appl. Phys.* **62**(6), 2545 (1987).
- R. H. Miles, D. H. Chow, J. N. Schulman, and T. C. McGill, “Infrared characterization of InAs/Ga<sub>1-x</sub>In<sub>x</sub>Sb superlattices,” *Appl. Phys. Lett.* **57**(8), 801 (1990).
- C. H. Grein, P. M. Young, and H. Ehrenreich, “Minority carrier lifetimes in ideal InGaSb/InAs superlattices,” *Appl. Phys. Lett.* **61**(24), 2905 (1992).
  - McGill SSDP Group Ph.D.s
  - McGill close collaborators

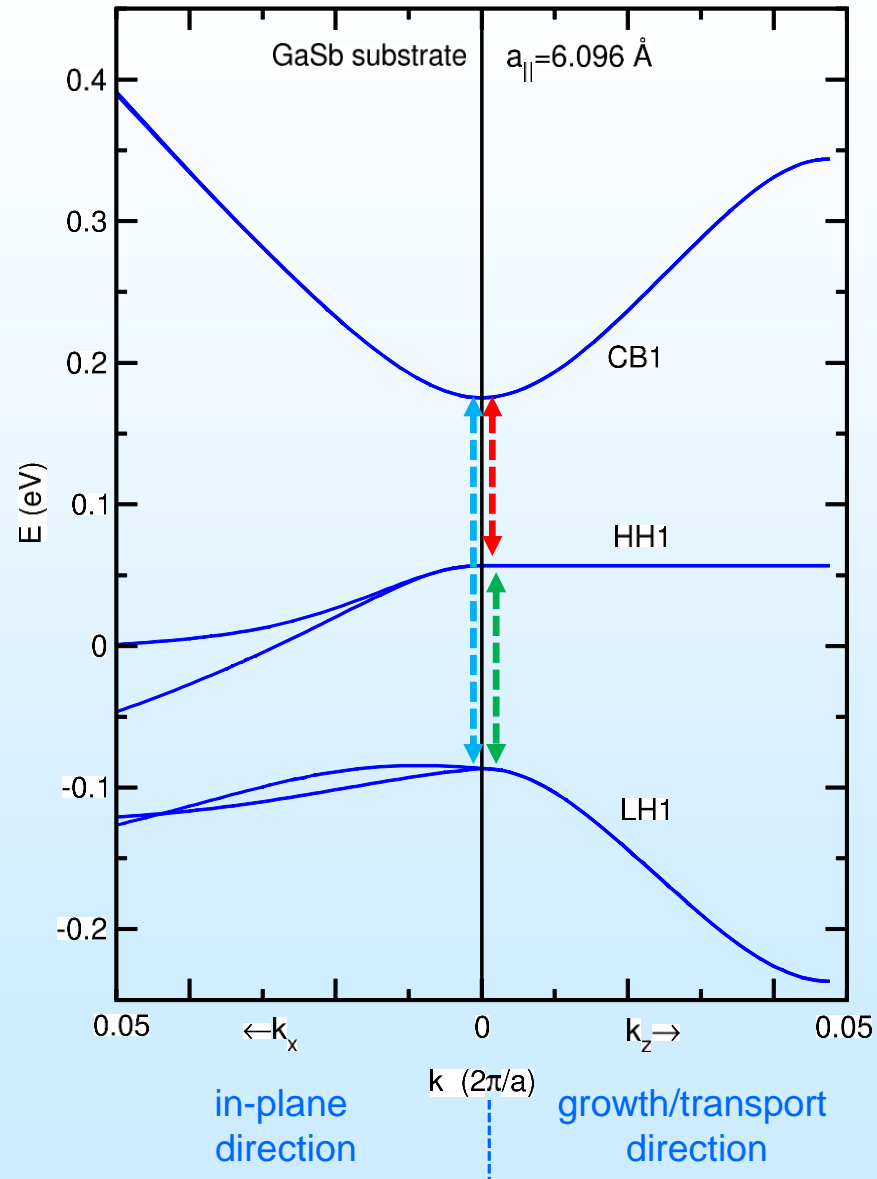
# Basic Properties of InAs/Ga(In)Sb Type-II Superlattice



- Type-II broken-gap superlattice
  - Spatially separated CB and VB wave functions
    - Reduced oscillator strength (compensated by larger VB edge density of states)
  - Type-II SL band gap is smaller than band gap of either bulk semiconductors
    - Type-I SL band gap always larger than the smaller bulk band gap
  - Nearly independent control of conduction and valence subband edges
    - Important for manipulating band alignments

# LWIR Superlattice Properties Deduced from Band Structure (1)

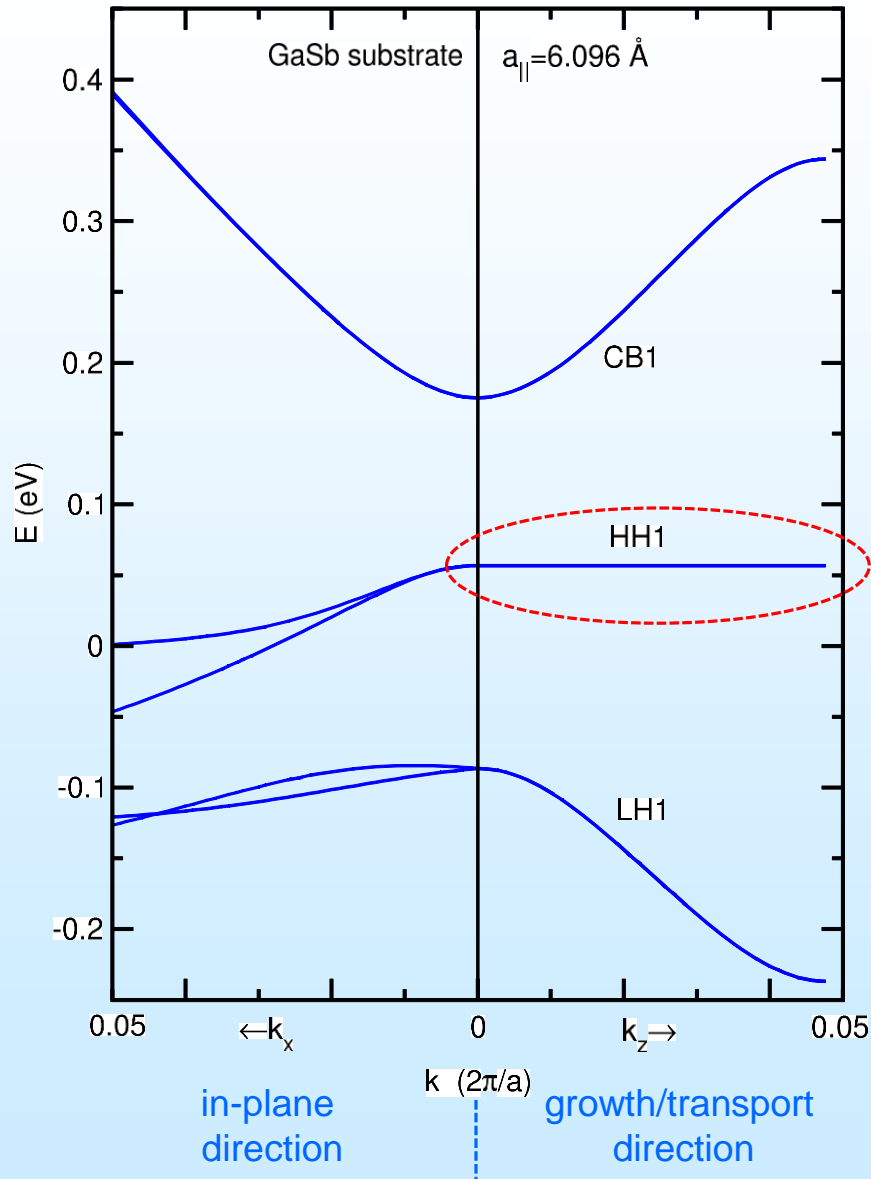
(14,7)-InAs/GaSb Superlattice



- Key features of LWIR SL band structure
  - Splitting of LH1 and HH1
  - Strong anisotropy in HH1 band
    - Low dispersion along growth/transport direction
- Absorption property
  - Cutoff wavelength determined by  $E_g = (E_{c1} - E_{hh1})$
  - Low dispersion in HH1 band along growth direction leads to larger VB edge (2D) density of states for enhanced absorption
    - Compensates for lower oscillator strength
- Reduced electron diffusion current
  - $m_c^*$  determined by  $(E_{c1} - E_{lh1})$
- Reduced tunneling leakage
  - Due to the larger  $(E_{c1} - E_{lh1})$
- Suppressed Auger recombination
  - $[(E_{hh1} - E_{lh1}) > E_g]$  favors Auger suppression
  - More easily attained in LWIR than MWIR

# LWIR Superlattice Properties Deduced from Band Structure (2)

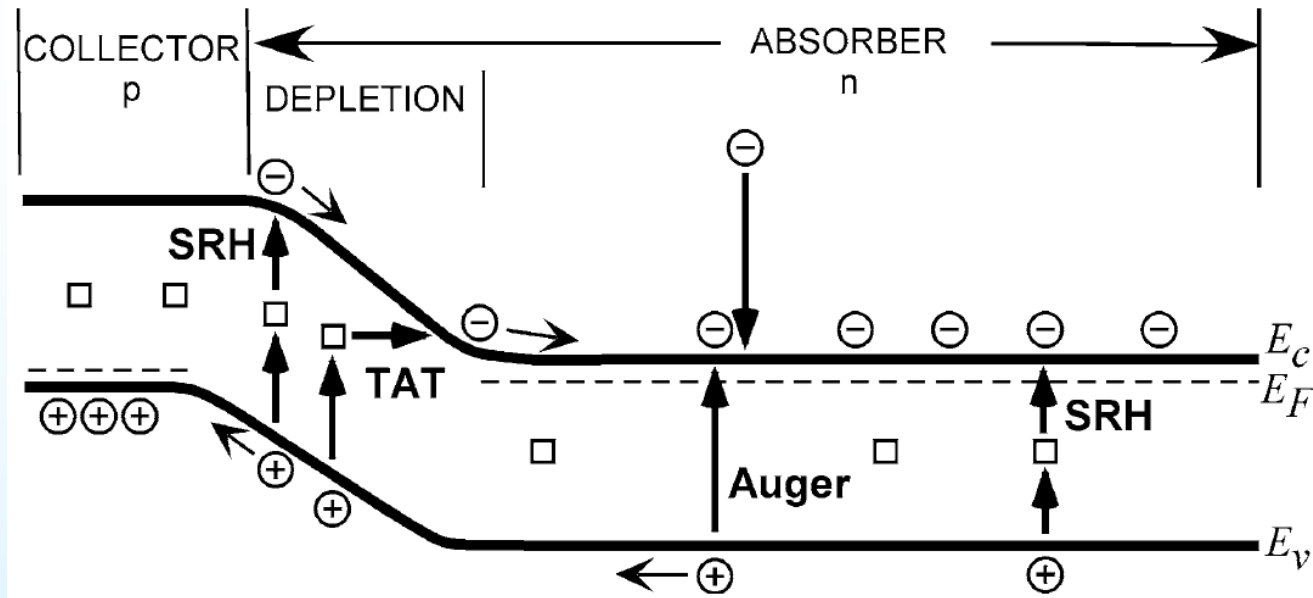
(14,7)-InAs/GaSb Superlattice



- Transport property

- Recall  $v_j = (1/\hbar)(\partial E/\partial k_j)$
- Good isotropic electron mobility
- Good in-plane hole mobility
  - Hole splitting; reduced scattering
- **Greatly reduced hole mobility along transport-direction**
  - Very large hh1 mass along growth direction
- Use **p-type LWIR superlattice** for more favorable minority carrier transport
  - Good (electron) diffusion length

# Dark Current Mechanisms in a Homojunction Diode



D. R. Rhiger, J. Electronic Materials, 40(8) 1815 (2011)

- High performance IR detector require good signal (photoresponse; QE) to noise (dark current) ratio
  - High QE achieved using thick, strain-balanced absorbers
- Dark current mechanisms in a p-on-n homojunction
  - Trap assisted tunneling, band-to-band tunneling
  - G-R current from SRH processes in depletion region
  - Diffusion dark current from Auger and SRH processes in quasi-neutral region
  - Surface leakage current (not shown)



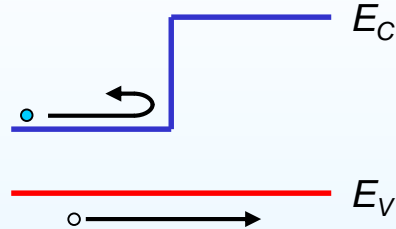
# G-R Dark Current Suppression using Unipolar Barriers

# Barrier Infrared Detector (BIRD)

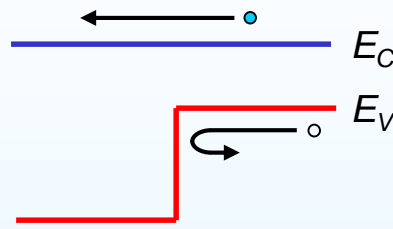
- Homojunction LWIR superlattice detectors have limited performance
  - p-n, p-i-n diodes
  - Good responsivity and QE
  - High dark current
- Designs based on heterostructures can enhance performance
  - Barriers can reduce dark current
  - But do not want to cut down responsivity/QE
  - “Unipolar barriers” are particularly useful in this respect

# Unipolar Barriers

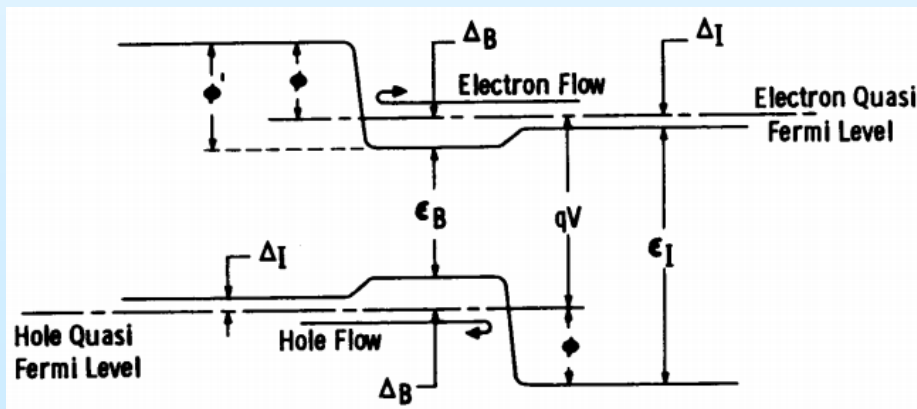
Electron blocking barrier



Hole blocking barrier

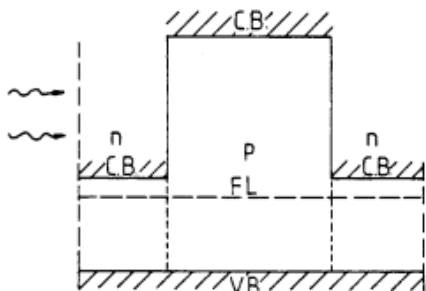


Double Heterostructure Laser



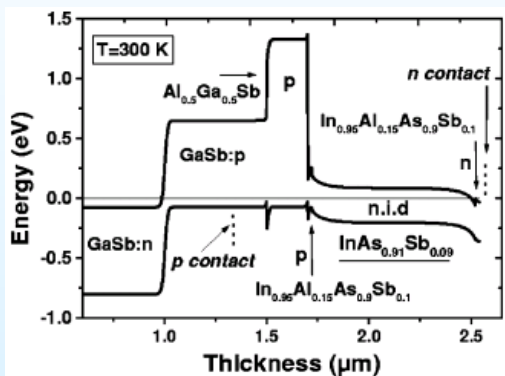
- Unipolar barriers:
  - Block one carrier type, but allows un-impeded flow of the other
  - Electron barrier
  - Hole barrier
  - Terminology introduced in Ting *et al. Appl. Phys. Lett.* **95**, 023508 (2009), now in common usage
  
- Using unipolar barriers to enhance semiconductor device performance
  - DH Laser, H. Kroemer, Proc. IEEE 1963
  - DH Laser, Zh. I. Alferov and R. F. Kazarinov, patent certificate (Russian) 1963

# Unipolar Barriers in Infrared Detectors

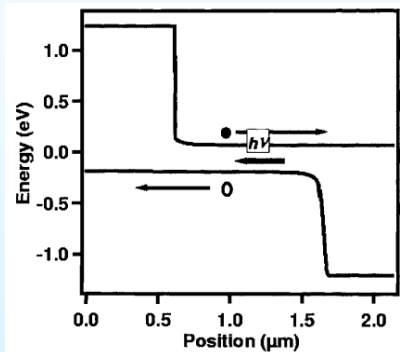


A.M. White,  
Patent, 1987

- Unipolar barriers can be used to enhance detector performance
  - Reduces SRH, surface leakage, and diffusion dark current
  - Enhances photo-generated carrier collection efficiency
  - Possible to reduce dark current without impeding photocurrent

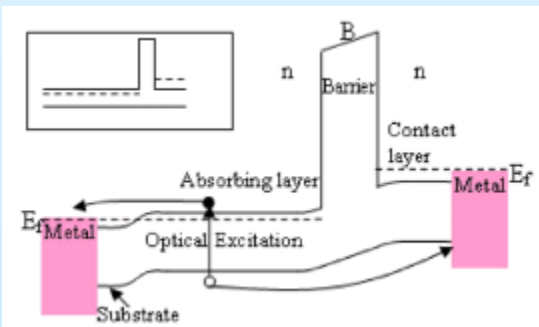


Rakovska et al, APL, 2000

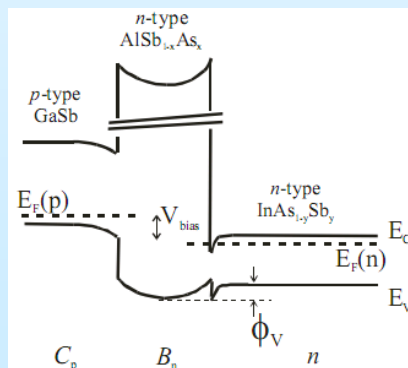


Carras et al, APL, 2005

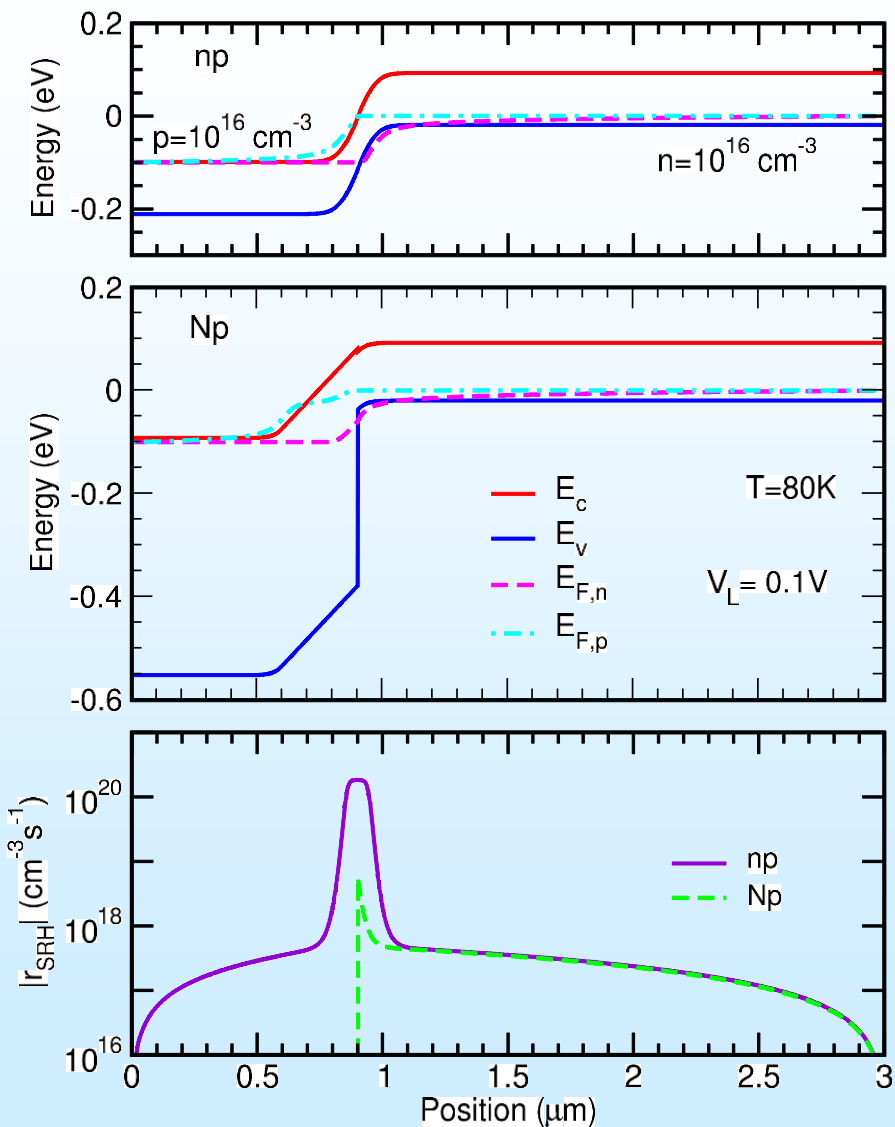
- Barrier infra-red detector (BIRD) examples
  - Unipolar barriers for impeding majority carrier current flow in photoconductors (A. M. White, 1983 patent)
  - Decreasing minority carrier concentrations on two sides surrounding the active absorber region, DH detector structure (Thales/Paris 7, APL, 2005)
  - Reduction of SRH surface leakage dark current, nBn (Maimon & Wicks, APL 2006), XBn (Klipstein, SPIE, 2008)



Maimon & Wicks, APL, 2006



Klipstein, SPIE, 2008

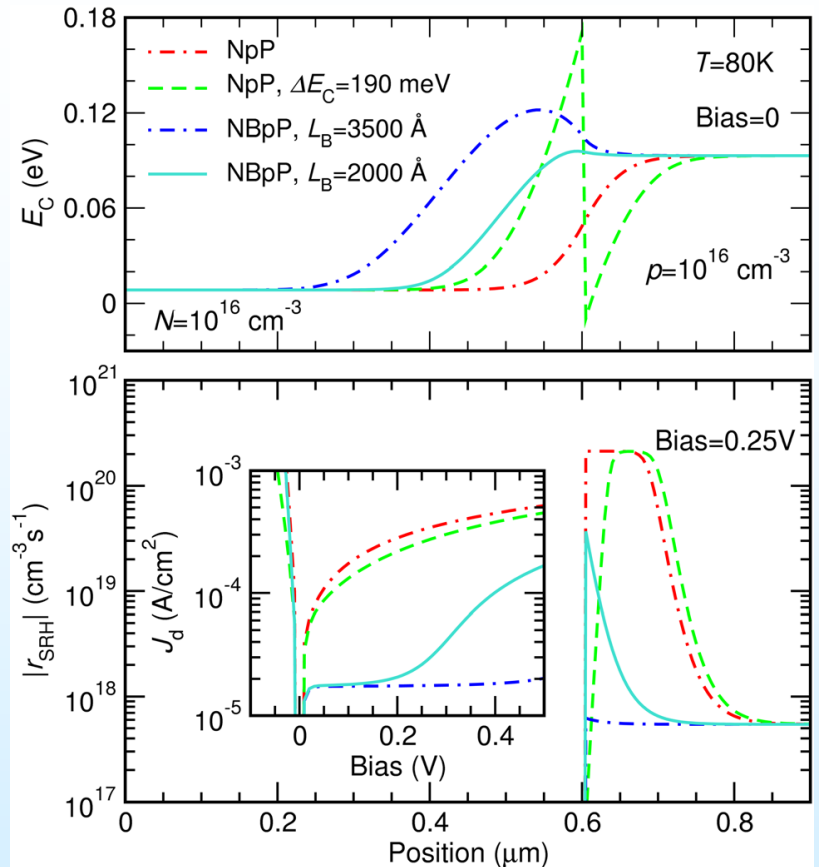
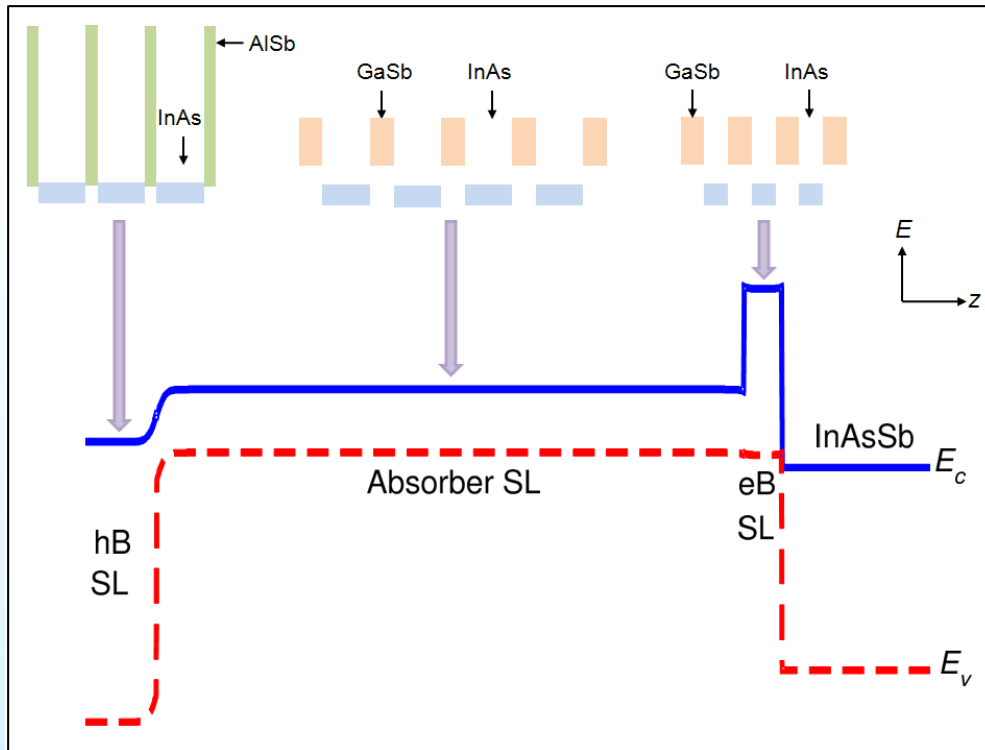


- Drift-diffusion simulation comparing LWIR SL np and Np diodes
- np homodiode
  - LWIR InAs/GaSb SL
- Np heterodiode
  - LWIR InAs/AlSb SL p-type absorber
  - InAs/AlSb SL hole-blocking unipolar barrier
  - Hole barrier does not block photocurrent
- SRH recombination rate given by
 
$$r_{SRH} = (np - n_i^2) / [(\tau_p (n + n_i) + (\tau_n (p + p_i)))]$$
- The Np heterostructure can be effective at SRH suppression



# Complementary Barrier Infrared Detector (CBIRD) Device and Focal Plane Arrays

# Junction Placement Effects in the CBIRD



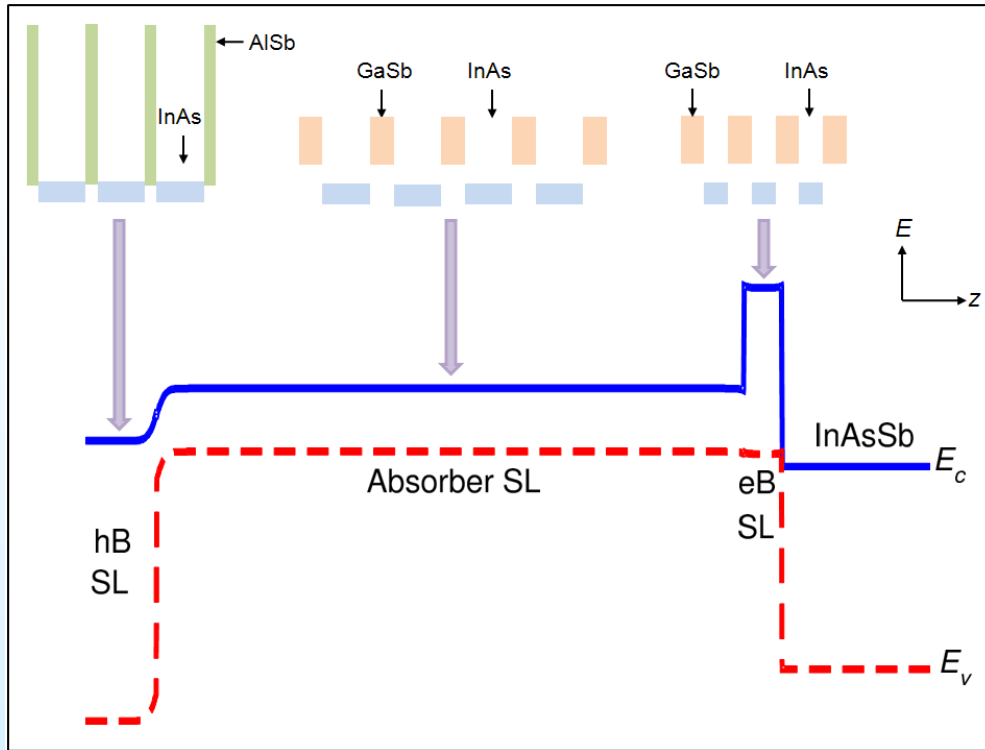
Calculated zero-bias conduction band (CB) profile near the hole barrier–absorber junction (located at  $0.6 \mu\text{m}$ ) for a set of structures with varying CB offset and doping profile (top panel), and the corresponding magnitudes of SRH generation-recombination rates under  $0.25\text{V}$  bias (bottom panel), with calculated J-V curves (inset).

- Complementary Barrier Infrared Detector (CBIRD)
- p-type LWIR superlattice absorber surrounded by
  - n-doped unipolar hole barrier (hB)
  - p-doped unipolar electron barrier (eB)
- Bottom tunneling contact

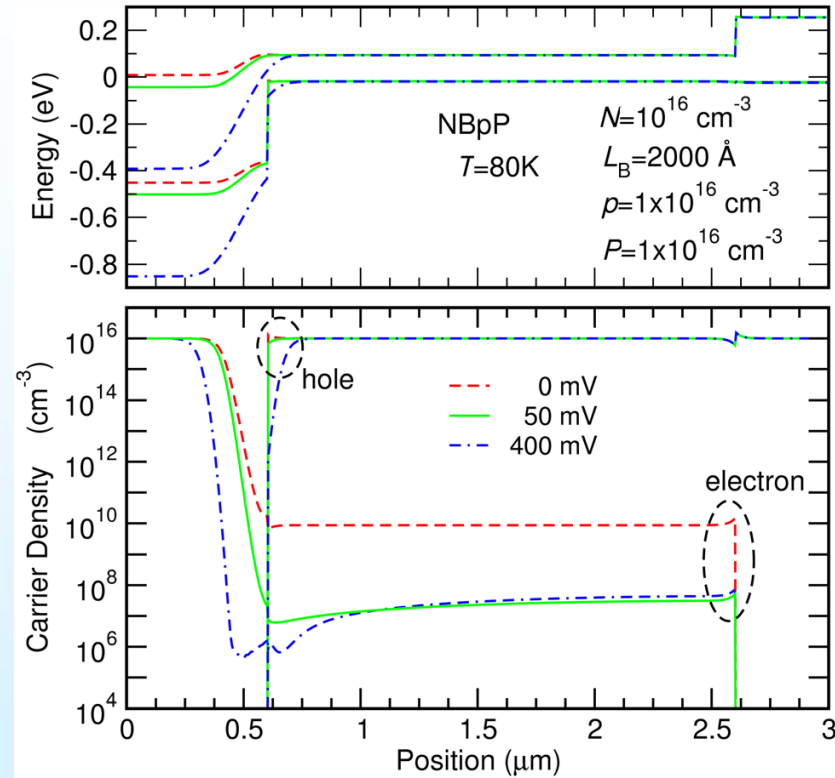
Ref: David Z.-Y. Ting *et al.*, “A high-performance long wavelength superlattice complementary barrier infrared detector,” *Appl. Phys. Lett.* 95(2), 023508 (2009).

Ref: D.-Z. Ting *et al.*, “Exclusion, extraction, and junction placement effects in the complementary barrier infrared detector,” *Appl. Phys. Lett.* 102, 121109, (2013)

# Carrier Exclusion and Extraction Effects in the CBIRD



Complementary Barrier Infrared Detector (CBIRD)



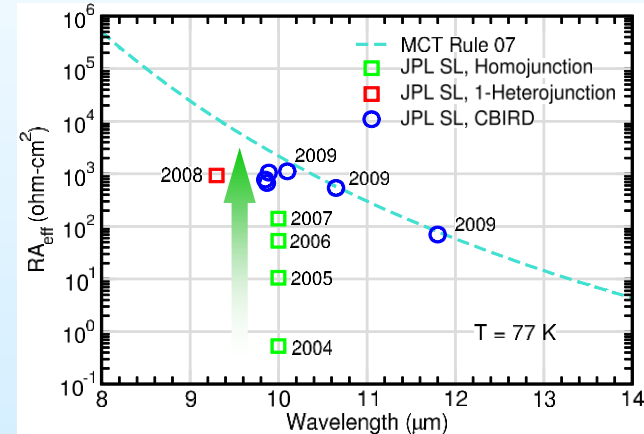
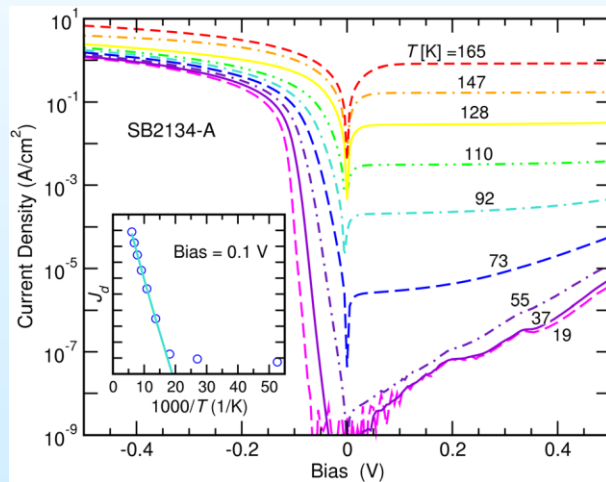
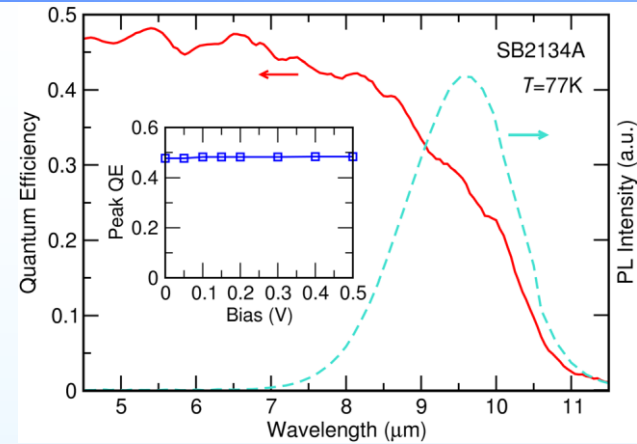
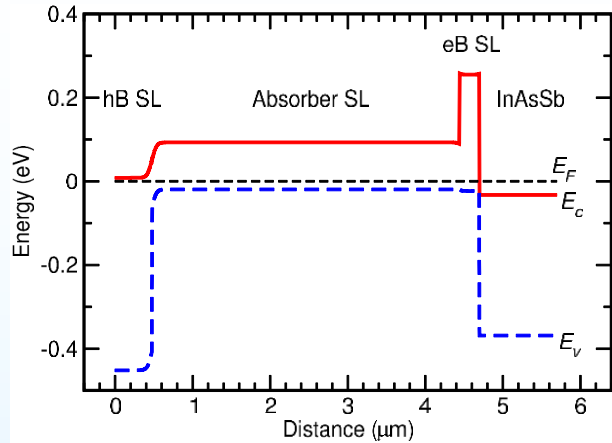
Calculated energy band diagrams (top panel) and carrier densities (bottom panel) for the active region of a CBIRD structure under various biasing conditions.

Exclusion, extraction, and junction placement effects in the complementary barrier infrared detector, D.-Z. Ting *et al.* Appl. Phys. Lett. **102**, 121109, (2013)



# CBIRD Device Structure & Single Pixel Data

Jet Propulsion Laboratory  
California Institute of Technology



Ref.: Tennant et al., J. Electron. Mat. 37, 1406 (2008)

- Fit  $J_d(0.1V, T)$  to diffusion-limited functional form:  $C T^3 \exp(-\Delta E/k_B T)$ 
  - Good fit down to below 77 K
  - The fitted value for  $\Delta E$  is 0.126 eV ; in good agreement with observed cutoff wavelength
- 10  $\mu\text{m}$  cutoff (50% peak responsivity)
- $R_0A = 14,000 \text{ ohm-cm}^2$  at 77 K, 10  $\mu\text{m}$  cutoff
- Dark current density under operating condition:  $J_{\text{dark}}(0.1V) = 0.989 \cdot 10^{-5} \text{ A/cm}^2$  at 77K



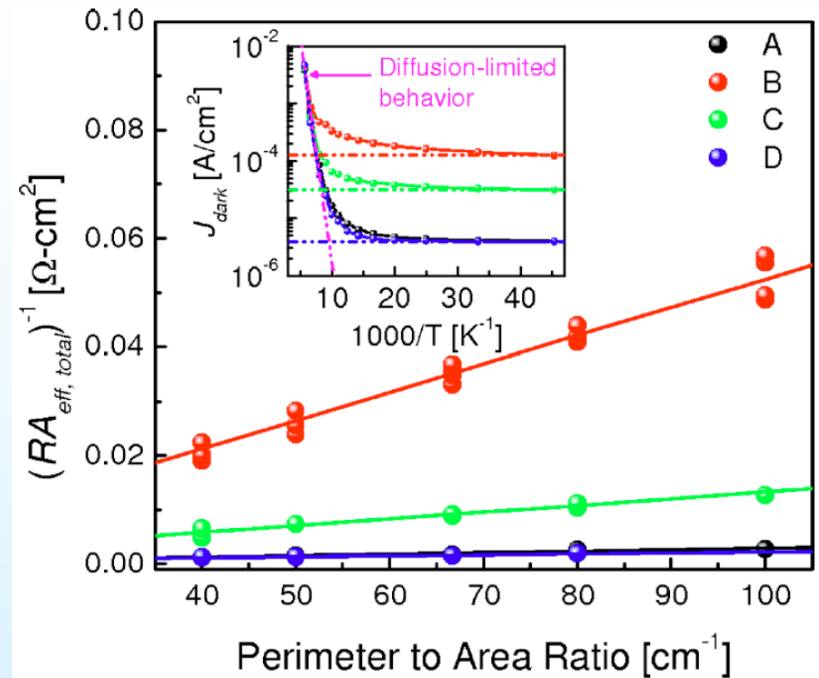
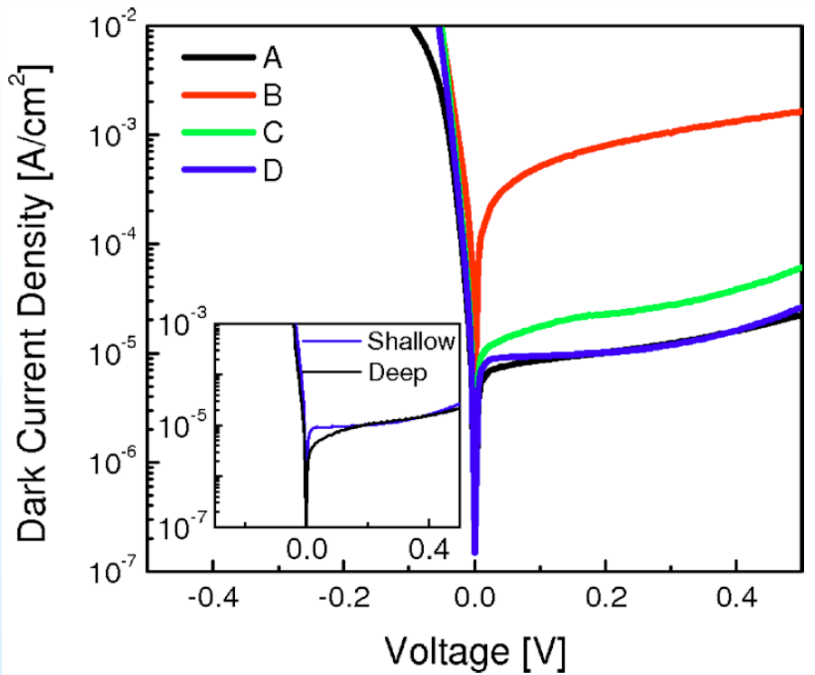
# Dry Etch Process Development

Jet Propulsion Laboratory  
California Institute of Technology

Sample	Type	Chemistry
A	Wet	$C_4H_6O_6:H_3PO_4:H_2O_2:H_2O$ ; citric clean
B	ICP Dry	$BCl_3$ /Ar plasma; citric clean
C	ICP Dry	$CH_4/H_2$ /Ar plasma
D	ICP Dry	$CH_4/H_2/BCl_3/Cl_2$ /Ar plasma

- Using a CBIRD sample containing
  - InAs/GaSb superlattices with ~2:1 InAs to GaSb ratio
  - InAs/GaSb superlattices with ~1:1 InAs to GaSb ratio
  - InAs/AlSb superlattice
  - Challenging
- Same sample etched by 4 different techniques

# Etching Experiment: Dark Current Results



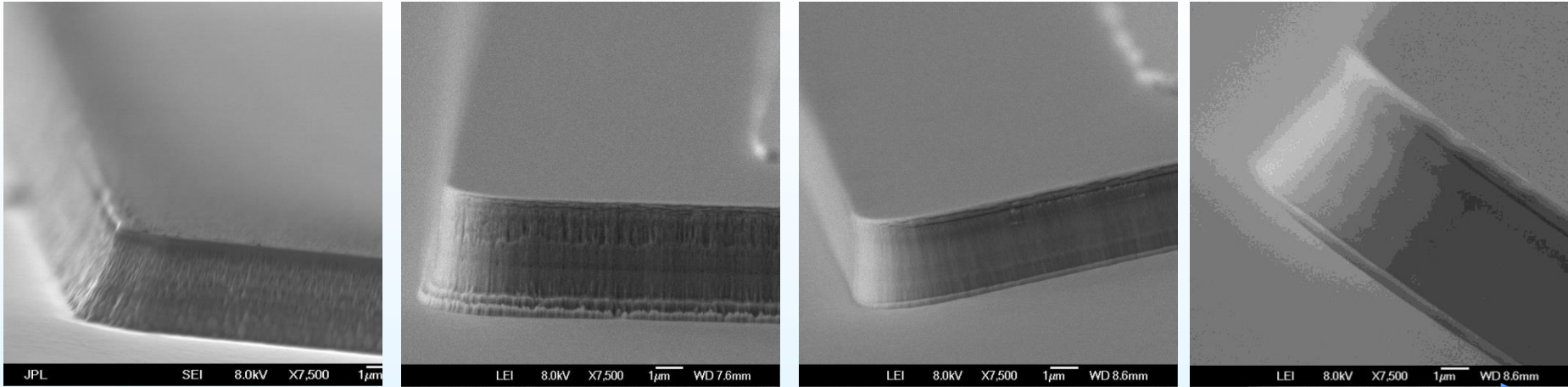
- Method D ( $\text{CH}_4/\text{H}_2/\text{BCl}_3/\text{Cl}_2/\text{Ar}$  ICP dry etch) produced dark current densities comparable to wet-etched devices (Method A)
- Deep and shallow etch (4:1 exposed surface area ratio) show similar dark current densities
- Variable device size study shows Method D produced the lowest surface-to-bulk dark current ratio

## Functions of the etch components

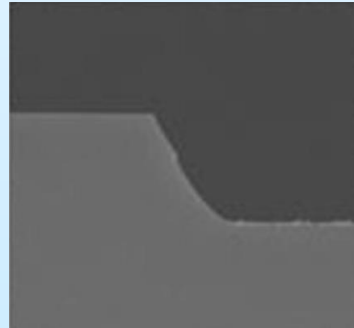
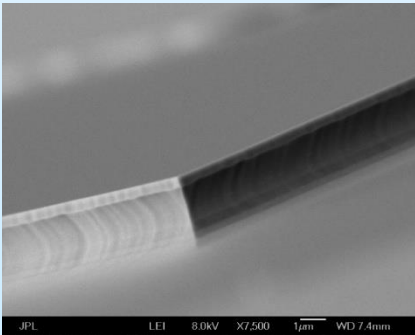
- Methane/hydrogen:
  - more effective indium removal allow lower etch temperature
  - promote the formation of a thin polymer pseudo-passivation layer
  - [A. Hood *et al.*, APL 2007]
- BCl<sub>3</sub>:
  - effective in removing unwanted native oxides and re-deposited byproducts
  - [A. Gin *et al.*, Thin Solid Films (2004)]
- Cl<sub>2</sub> (slight amount):
  - increase the etch rate
  - reduce erosion of the SiN<sub>x</sub> hard mask
- Can be tuned to achieve very similar etch rates for InAs, GaSb, AlSb, and InAsSb layers

# Dry Etching Progress at JPL

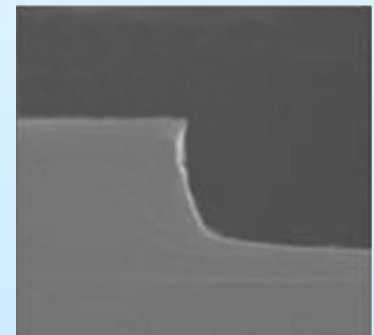
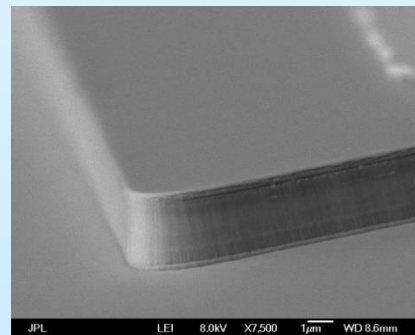
All dry etching consisted of the same parameters used to etch the entire structure



- QWIP recipe
- Optimization for p-i-n
- Optimization for CBIRD
- Remove the need for wet etch clean up
- Tweak for 17.5 µm pitch FPAs



Wet Etching



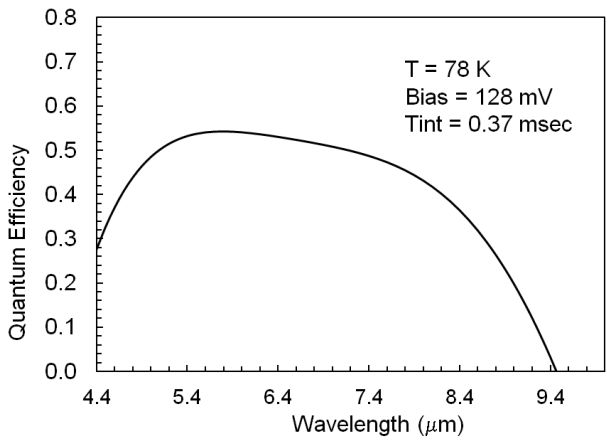
Dry Etching

Dry Etching resulted in 8.2° sidewalls compared to 35.1° from wet etching



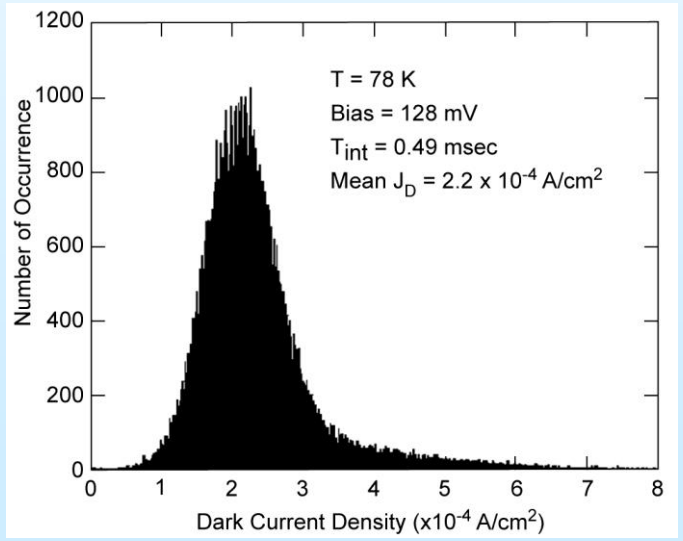
# LWIR CBIRD FPA

Jet Propulsion Laboratory  
California Institute of Technology



Single Pixel QE

Format	– 320x256
Pixel pitch	– 30 $\mu\text{m}$
ROIC	– ISC 0903 DI
Pixels	– Fully reticulated
Pixel Size	– 26x26 $\mu\text{m}^2$
Polarity	– N on P
Cutoff wave.	– 10 $\mu\text{m}$
Oper. temp.	– 78 K
QE (8-9.2 $\mu\text{m}$ )	– 54% (without A/R)
NE $\Delta T$	– 18.6 mK with f/2 300K
Substrate	– Removed
Temp. Cy	– 29

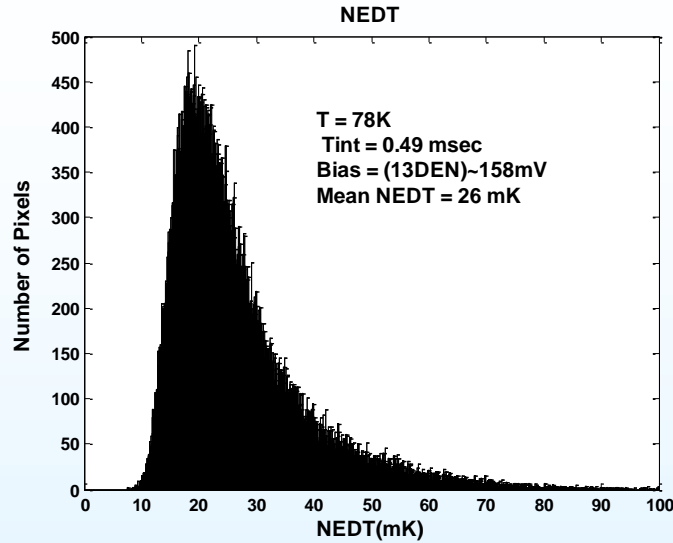


Dark Current Density





1/4 VGA Video



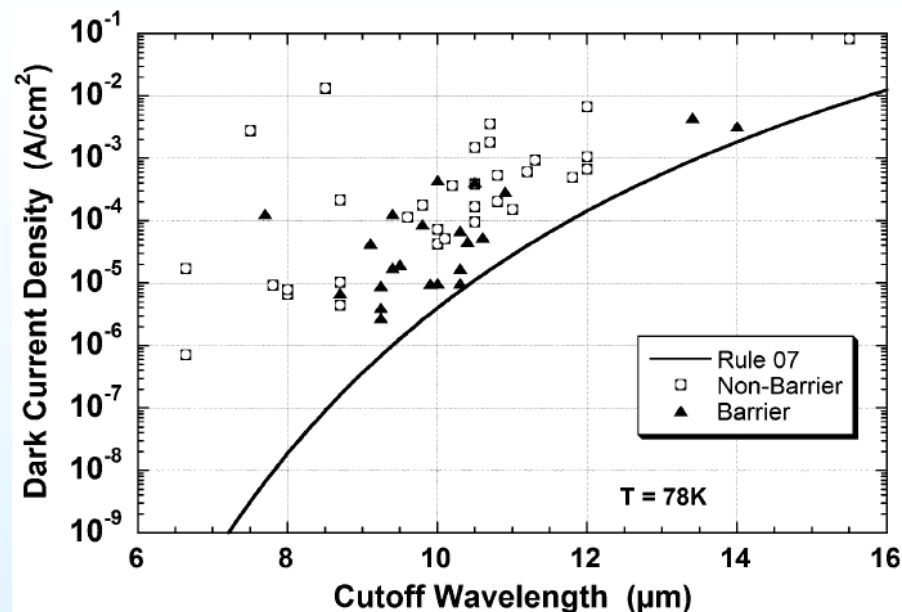
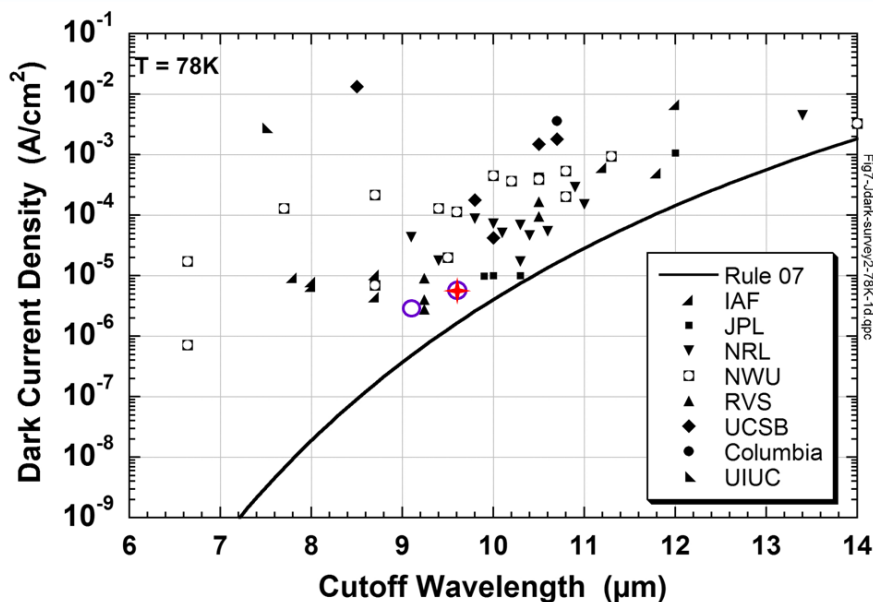
Format – 320x256  
Pixel pitch – 30 mm  
Polarity – N on P  
Cutoff wavelength – 10.2  $\mu\text{m}$   
Operating temp. – 80K



1Kx1K Image

Superlattice Characteristic	Advantage	Tangible Benefit to FPAs
Band structure engineering	Suppress Auger related dark current	High operating temperature
Large electron effective mass	Smaller leakage currents	High SNR
Interband transitions	Normal incidence absorption	High quantum efficiency (fast arrays)
Adjustable bandgap	Tunable wavelength from visible to 24 $\mu\text{m}$	Multicolor capability
III-V semiconductor based	Strong bonding	High uniform, Low cost, Robust

# Dark Current Performance of Published Superlattice Detectors



Published SL photodiode dark current densities as of late 2010. [D. R. Rhiger, *J. Elect. Mat.* **40**, 1815, (2011)]

- Single element superlattice detector dark current performance approaching Rule 07
  - Including devices using material from commercial growth foundries
- Unipolar barriers enhance dark current performance

# Modulation Transfer Function (MTF)

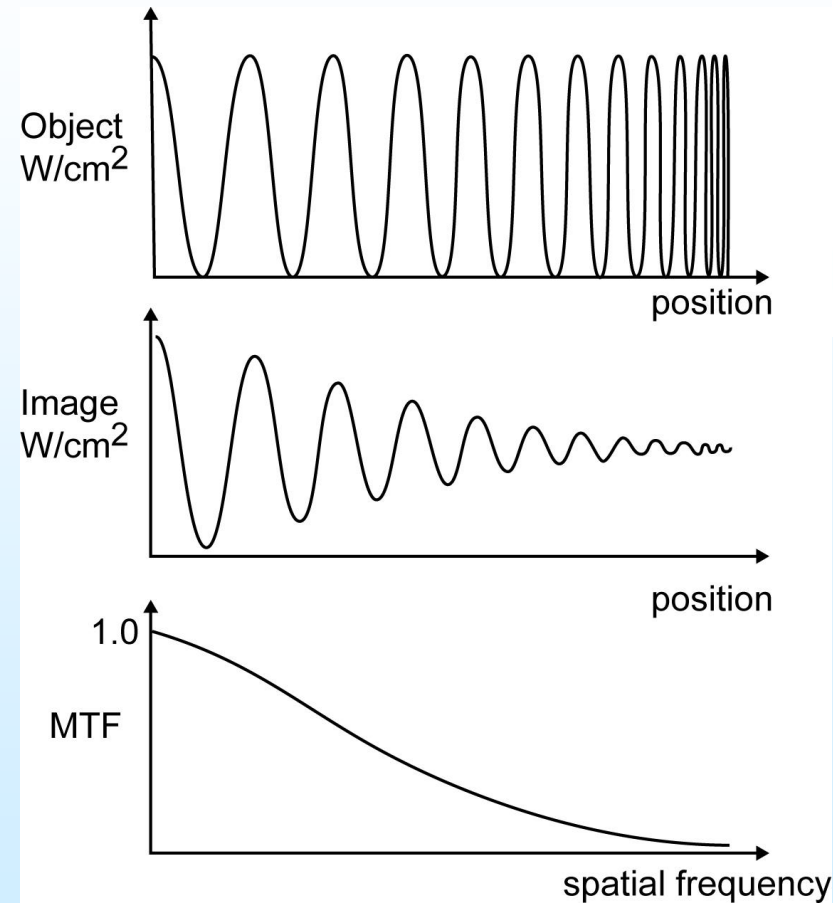
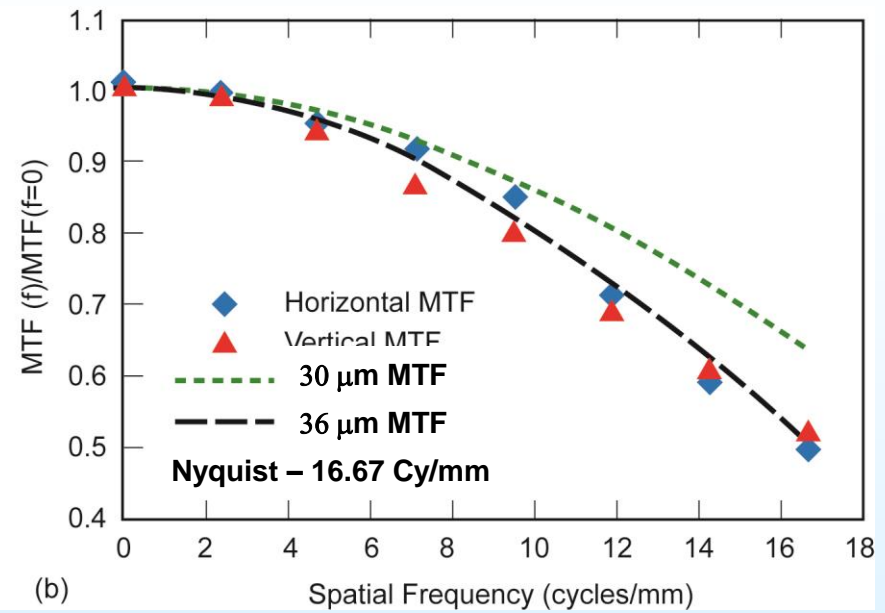
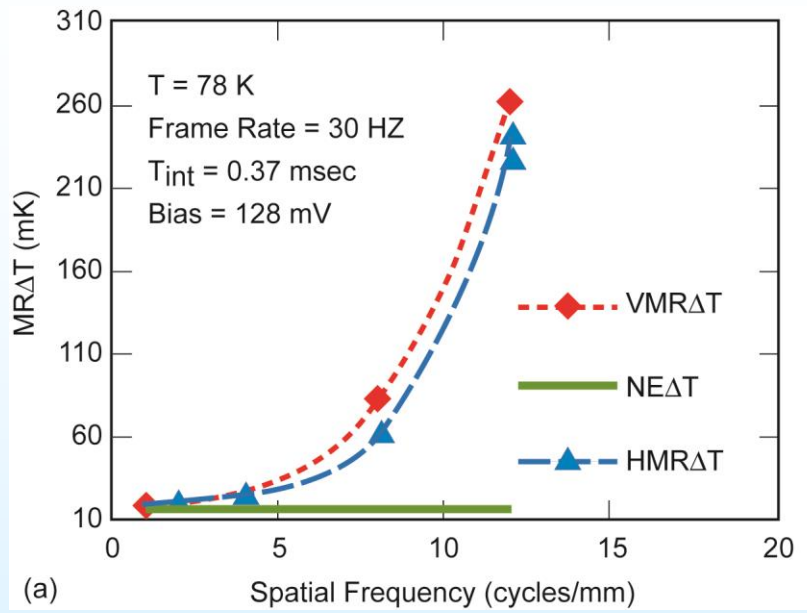


Image at left has a higher pixel count than the one to the right, but is still of worse resolution due to poor MTF



# MTF of LWIR CBIRD FPA

Jet Propulsion Laboratory  
California Institute of Technology



HMTF and VMTF are FPA MTF (i.e., lens MTF removed)  
 Lens MTF = Sinc X = (SinX)/X where X = Pixel Pitch. $\pi$ . (Spatial Frequency/Cutoff Frequency)  
 Cutoff Frequency =  $1/\lambda \cdot f/\#$   
 Ideal MTF plot is Sinc 30  $\mu\text{m}$  for 30  $\mu\text{m}$  pixel pitch  
 Data show MTF closer to Sinc 36  $\mu\text{m}$  for 36  $\mu\text{m}$  pixel pitch  
 Ideal MTF at Nyquist frequency ( $\sim 16.67$ cycles/mm) is 0.64  
 At Nyquist frequency vertical and Horizontal MTF has a value of  $\sim 0.48$  and 0.50 respectively



# Lifetime and Diffusion Dark Current

# Short Lifetime but Low Dark Current

- LWIR SL lifetime  $\sim 30$  ns (77K)
  - 31 ns for LWIR SL;  $>1$   $\mu$ s for MCT (optical modulation response)
    - SRH dominant
    - [D. Donetsky et al., APL 97, 052108 (2010); Stony Brook]
  - 35 ns (dark current analysis)
    - [J. Pellegrino & R. DeWames, SPIE 7298 (2010); NVESD]
  - 30 ns (time resolved PL decay)
    - [Connelly et al., APL 97, 25117 (2010); ARL]
  - 33-38 ns for LWIR SL (optical modulation response)
    - [L. Höglund et al., *Proc. SPIE* **8511**, 8511-6 (2012); JPL]
- Substantially shorter lifetime than MCT
- But CBIRD dark current is near diffusion limited, and within a factor of a few of MCT Rule '07
- How is this possible?

# Diffusion Dark Current and Lifetime

- LWIR ( $\lambda_c \sim 10 \mu\text{m}$ ) CBIRD dark current characteristics
  - Near diffusion limited behavior, down to below 70K
  - Dark current level approaching MCT Rule ' 07
- Diffusion dark current (p-side)

$$J_{e,diff} = qn_0L / \tau_n$$

- $L$  : diffusion length (or absorber width)
  - $\tau_n$  : minority carrier lifetime
  - $n_0$  : minority carrier density
- Under (quasi-) equilibrium conditions

$$J_{e,diff} = qn_i^2 L / (N_a \tau_n)$$

- Related to acceptor doping level  $N_a$

# Doping, Lifetime, and Dark Current

- Reduced tunneling in SL permits higher absorber doping than in MCT
  - Typical LWIR SL doping level:  $p = 1 \text{ to } 2 \times 10^{16} \text{ cm}^{-3}$
  - Typical LWIR MCT doping level:  $n = 1 \times 10^{15} \text{ cm}^{-3}$

- Higher doping compensates for shorter lifetime in SL
  - Recall diffusion dark current from p-type absorber given by

$$J_{e,diff} = qn_i^2 L / (N_a \tau_n)$$

- Higher doping leads to lower equilibrium minority carrier density
- Larger superlattice  $m_c^*$  also reduce diffusion current in p-type absorber



# Summary

Jet Propulsion Laboratory  
California Institute of Technology

- The antimonide material system provides
  - Added material robustness for manufacturability
  - Variety of band offsets for flexibility in design
  - Large-area substrates for large format arrays/economy of scale

## InAs/GaSb Superlattice

- Quantum efficiency
  - High quality, thick samples show good QE
- Tunneling dark current
  - Intrinsically reduced in superlattice
- G-R dark current
  - Suppressed by unipolar barrier based designs such as CBIRD
- Diffusion dark current
  - Effect of short lifetime compensated in part by higher doping density
    - permitted by reduced tunneling in superlattice
  - Need to **increase lifetime** to reach promised potential
- Surface leakage dark current
  - Shallow etch: Leave narrow gap absorber un-exposed
  - Deep etch: surface leakage minimized with a combination ICP dry etch
- Excellent progress towards high-performance superlattice FPAs

# Key Properties of Type-II Superlattices

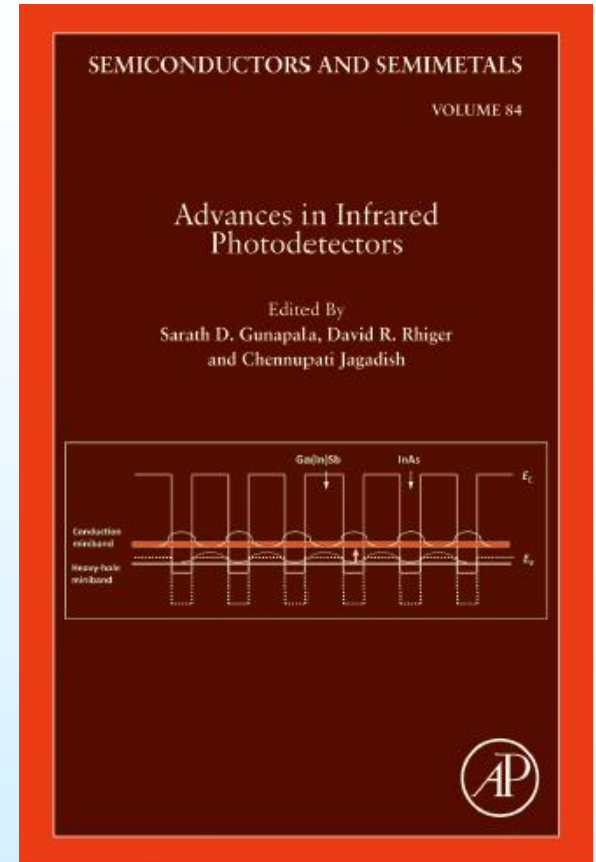
- Infrared band gap from SWIR to VLWIR
- Absorption strength comparable to MCT
- Strain-balanced thick absorber provides ample QE

## Advantages:

- Lower tunneling leakage
- Reduced diffusion dark current (p-type)
- **Reduced Auger** generation
- Large area substrates (economy of scale)

## Challenges:

- G-R dark current induced by **SRH** processes
- Lifetime significantly lower than MCT
  - Attributed to **SRH**
  - Effect of short lifetime on diffusion dark current
- Surface leakage

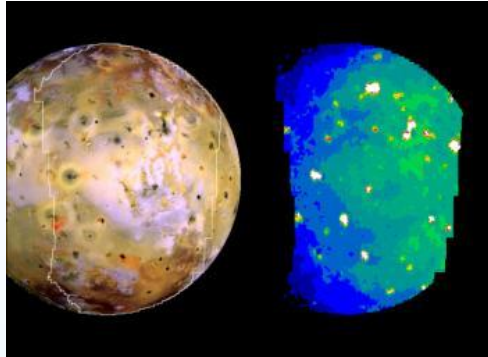


“Type-II Superlattice Infrared Detectors”,  
D. Z. Ting, A. Soibel, L. Höglund,  
J. Nguyen, C. J. Hill, A. Khoshakhlagh,  
and S. D. Gunapala,  
*Semiconductors and Semimetals* **84**,  
pp.1-57 (2011).



# NASA Applications

# Ultra-High Dynamic Range Multi-Spectral IR Imager



Io in infrared (right) at 4.7  $\mu\text{m}$  showing multiple hot spots as seen by *Galileo* NIMS, NASA/JPL/UA. The brightest hot spots saturated the detectors, a major problem for imagers viewing Io's volcanoes.

**Our proposed instrument will solve this problem**

## Objective

- The overall objective of the proposed effort is to develop and demonstrate a large format (1280x480 pixels) multispectral (10 channels) Infrared Imager covering 1-10 $\mu\text{m}$  spectral range with very high thermal sensitivity (better than 1% of the scene temperature) and exceedingly high dynamic range (> 100dB SNR)

- The proposed imager will allow acquisition of **unsaturated** high spatial resolution SWIR/MWIR/LWIR images of Io's surface
  - Novel breakthrough digital read-out integrated circuit (ROIC) technology avoids well saturation, **providing an exceptionally high dynamic range, vital for observing Io's volcanoes and surfaces**
  - The advantage of the proposed imager compared to current thermal imagers such as the Diviner instrument are: 1) extremely high dynamic range capability to measure the wide range of temperatures; 2) imaging capability (1240x480) to cover large surface areas at high spatial resolution
- Fundamental science hypotheses: Broad IR coverage of Io obtaining unsaturated data to determine eruption temperature, map temperature range, and test internal heating models.

## Core Team

Team Member	Role	Org
A. Soibel	PI, Technical Lead	38
S. Gunapala and D. Ting	Co-I, FPA/Camera	38
A. Davies and P. Hayne	Co-I, Science	32
M. W. Kelly	Co-I, Electronics (DROICs)	MIT/LL

Technology Development Risk(s)	How Mitigated or Retired through Homesteader
Imager performance can degrade after exposure to radiation	Test radiation tolerance of the imager at the conditions relevant to Io mission
Camera performance can degrade after exposure to vibration and thermal-cycling	Environmental test of integrated dewar cooler assembly
Electronic board may have problems with control of digital ROIC	Test electronics operation in integrated assembly

# Thermal IR Camera for Hazard Detection, Avoidance, & EDL

## Chryse - Day / Night IR

THEMIS Night Time IR - 3 am



THEMIS Day Time IR - 3 pm

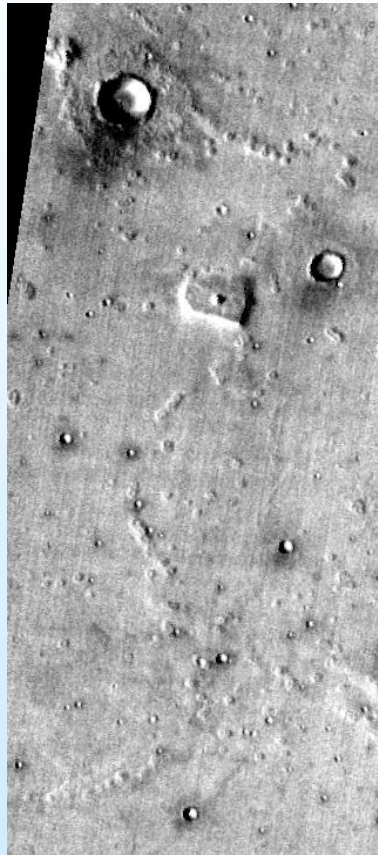
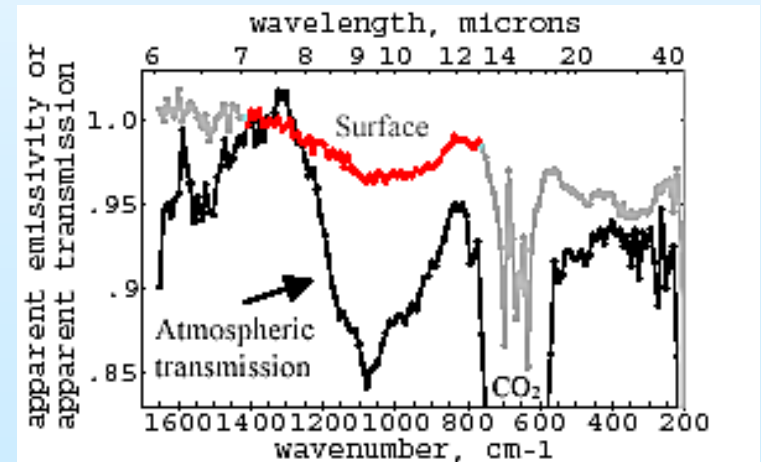


## Image Taken with QWIP Camera



Dec., east-looking, 0.5m rocks, 4pm

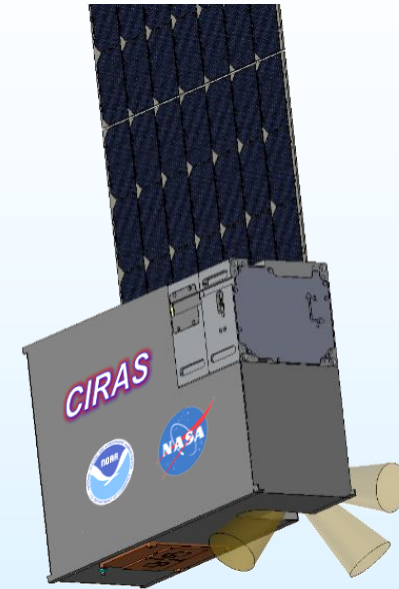


Atmospheric Transmission of Mars

# Atmospheric IR Sounder (AIRS)



AIRS Instrument based on HgCdTe detectors (2002)

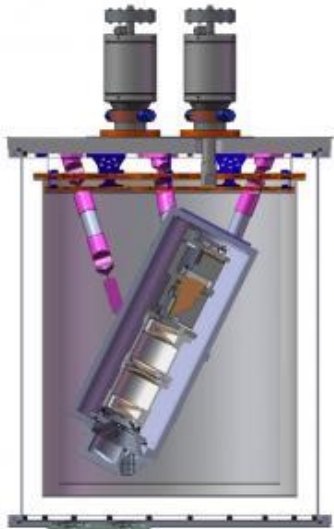


CIRAS Instrument (2018 – 6U cubesat) based on Antimonides CBIRD

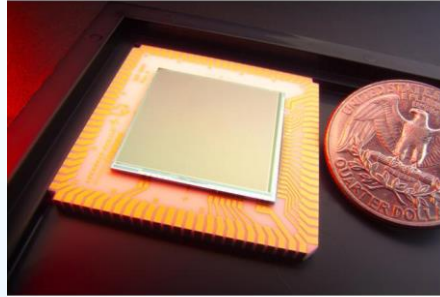


# Hyperspectral Thermal Emission Spectrometer (HyTES)

Jet Propulsion Laboratory  
California Institute of Technology



HyTES Instrument



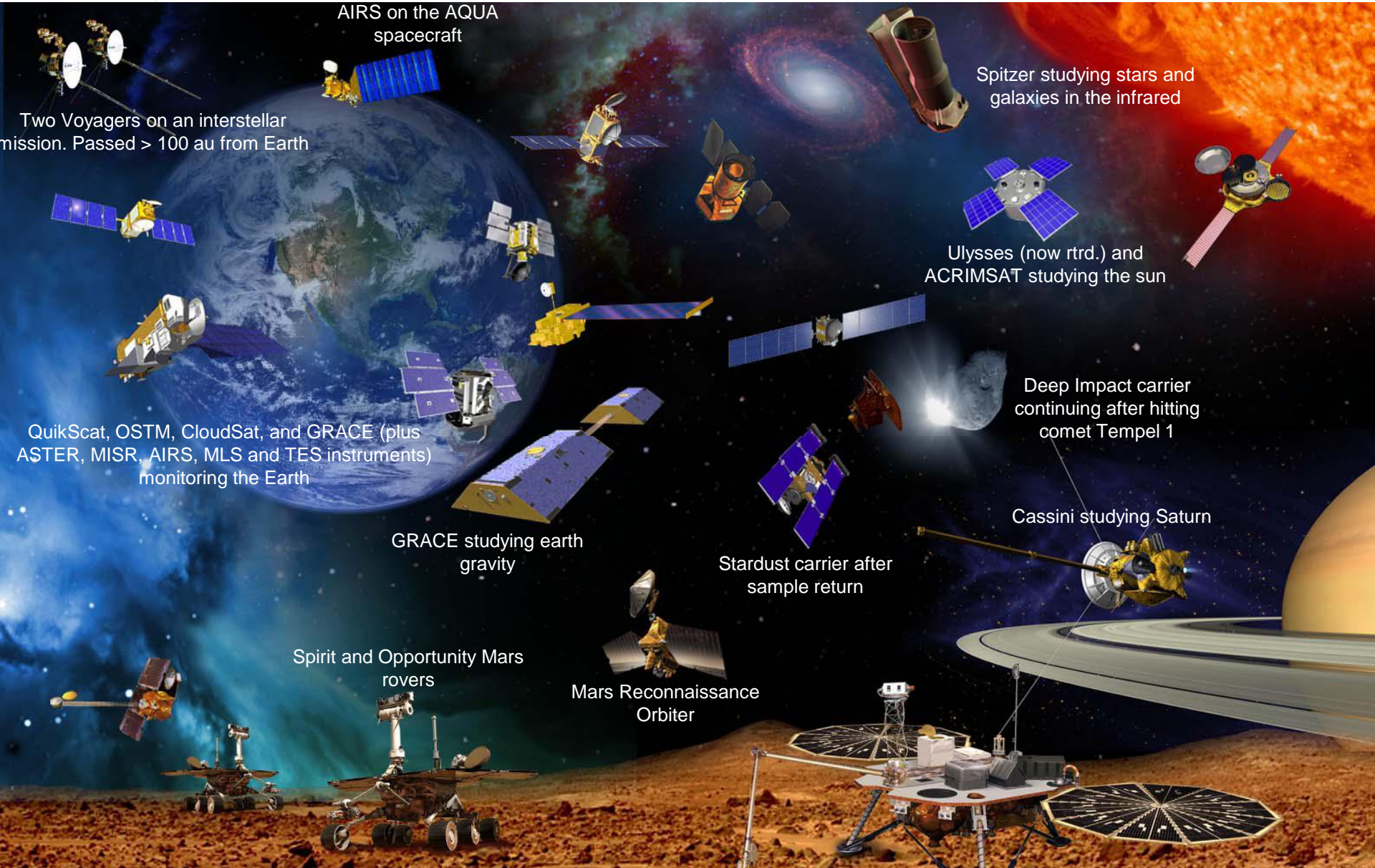
Based on 1Kx1K nine-band QWIP Focal Plane Array



Airborne HyTES Instrument

Spectral coverage	– 7.5-12 $\mu\text{m}$
Spectral channels	– 256 (17.6 nm)
Field of view	– 48.3
I FOV	– 1.44 mrad
Spatial elements	– 512
Pixel size at 2000m flight altitude	– 3.64 m
Slit width	– 39 $\mu\text{m}$
F-number	– 1.6

# 24 robotic spacecraft and 7 instruments across the solar system and beyond.....



Two Voyagers on an interstellar mission. Passed > 100 au from Earth

AIRS on the AQUA spacecraft

Spitzer studying stars and galaxies in the infrared

Ulysses (now rtrd.) and ACRIMSAT studying the sun

QuikScat, OSTM, CloudSat, and GRACE (plus ASTER, MISR, AIRS, MLS and TES instruments) monitoring the Earth

Deep Impact carrier continuing after hitting comet Tempel 1

GRACE studying earth gravity

Stardust carrier after sample return

Cassini studying Saturn

Spirit and Opportunity Mars rovers

Mars Reconnaissance Orbiter